TOPICAL REVIEW • OPEN ACCESS

Graphene aerogels: a review

To cite this article: George Gorgolis and Costas Galiotis 2017 *2D Mater.* **4** 032001

View the article online for updates and enhancements.

Related content

- Preparing three-dimensional graphene architectures: Review of recent developments
  Zeng Min, Wang Wen-Long and Bai Xue-Dong

- Graphene based 2D-materials for supercapacitors
  Thangavelu Palaniselvam and Jong-Beom Baek

- Phosphorene for energy and catalytic application—filling the gap between graphene and 2D metal chalcogenides
  Rishabh Jain, Rekha Narayan, Suchithra Padmajan Sasikala et al.

Recent citations

- Shamik Chowdhury *et al*

- Materials-by-design: computation, synthesis, and characterization from atoms to structures
  Jingjie Yeo *et al*

2D Materials

TOPICAL REVIEW

Graphene aerogels: a review

George Gorgolis[1] and Costas Galiotis[1,2]

[1]   Department of Chemical Engineering, University of Patras, Rio, 26504 Patras, Greece
[2]   Foundation of Research for Technology/Institute of Chemical Engineering Sciences (FORTH/ICEHT), Platani, 26504 Patras, Greece

E-mail: c.galiotis@iceht.forth.gr

Abstract

Graphene based aerogels (GAs) are 3D scaffold materials that can be lighter than air. Due to their fascinating properties, such as, high mechanical strength and electrical conductivity, thermal resistance and adsorption capacity, they have attracted a lot of interest currently. This review, covers the main routes for obtaining GAs namely, hydrothermal reduction/self-assembly, chemical reduction, template-directed reduction, cross-linking and sol–gel processes. Potential application fields for example in energy storage and environmental protection are also discussed. Finally, the future prospects of this exciting field based on the results published so far are examined.

Abbreviations

Gas	Graphene based aerogels
GO	Graphene oxide
rGO	Reduced graphene oxide
RTFG	Room temperature freeze gelation
CNTs	Carbon nanotubes
MWCNTs	Multiwalled carbon nanotubes
UGA	Unidirectional graphene aerogel
RT	Room temperature
LIBs	Lithium-ion batteries
GOA	Graphene oxide aerogel
PCM	Phase change material
GNS	Graphene nanosheets
3D	Three-dimensional
2D	Two-dimensional

1. Introduction

Graphene has been the focus of intense interest since its discovery in 2004 due to its excellent electrical, thermal and mechanical properties [1]. In particular, properties such as its high strength/strain-to-failure [2], high surface area [3] and chemical stability [4] have found applications in composites [5, 6], nanoelectronics [7, 8], energy storage [9, 10], sensors [11, 12], catalysis [13] and biomedicine [14]. Often, however, when graphene is encapsulated into polymers, the properties of the produced composites are lower than theoretical predictions [15–24]. This has been attributed to poor dispersion of graphene in the polymeric matrices

and the resulting agglomeration due to π–π stacking interactions between graphene sheets. In all cases, in order to fully exploit the properties of graphene certain methodologies must be devised to convert the 2D material to 3D structures. Thus it is very important to prepare and characterize graphene materials with three dimensional (3D) structure such as aerogels, hydrogels and macroporous films. Out of these structures, the aerogels show a great promise and have been investigated intensely [25–35]. It suffices to say that these materials show higher electrical conductivity than those which have been prepared by dispersion of graphene sheets [23, 36, 37]. Also, Graphene Aerogels can become lighter than air, and this is the reason why graphene has been proposed as a substitute for the relatively rare and expensive helium [38].

Aerogels, which are prepared from molecular precursors by sol–gel methods and followed by drying (freeze or supercritical) to remove the solvents from the wet gels and substitute with air, are porous nanomaterials that exhibit high surface area, tunable porosity and large pore volumes. Aerogels can exhibit high porosity (90–99%), low density (3 kg m^{-3}), low thermal conductivity (0.014 W m$^{-1}\cdot$K^{-1} at room temperature), low refractive index and low dielectric constant [39]. Thus, they can be applied in catalytic processes, electronic devices, Cerenkov detectors and other fields [40]. An important class of aerogels is carbon aerogels which are materials that can be used in a variety of applications [41, 42]. The porosity of the carbon aerogels can be controlled by the size and shape of the precursor nanoparticles since micropores are connected to the

intra-particle structure, while meso- and macropores are connected to the inter-particle structure [43].

Generally, graphene oxide (GO) is the appropriate precursor to prepare 3D graphene assemblies due to its high dispersion in aqueous media and its functionality. Also, GO is very useful as starting material in synthesizing graphene based aerogels (GAs), because the oxygen moieties that are present at both basal planes and edges are able to react covalently with different compounds and thus yield new materials with properties that can be tailored to specific applications. Among these compounds, biopolymers can be immobilized covalently onto GO sheets and that enhances their biocompatibility without affecting their overall performance. It has been shown that GO can be reduced to graphene via a hydrothermal process or by appropriate reducing agents yielding (by self-assembly) a 3D structure with pore sizes in the sub-micron to micron range [33]. The self-assembly is believed to take place due to hydrophobic interactions and π–π stacking between the reduced sheets. Very often, however, the resulting aerogel suffers from extreme brittleness. Consequently, a GA is a porous-low density-material that consists of a network of graphene aggregated sheets and which exhibited a relatively high, mechanical strength [44, 45].

GAs, due to their high surface area, high porosity, high specific capacitance and high cyclic stability, are anticipated to be used in energy storage as electrodes for electrochemical power sources and LIBs [46–48], as supercapacitors [49–51], in waste removal [52–54] and gas sensing [55–59] applications. They can also be used in air purification and as solar light photocatalysts [60], and as phase change materials for better heating-cooling responses [61]. Very often, the application possibility of GAs is increased thanks to nanoparticle addition, which enhances their already remarkable properties [47, 60, 62]. Nitrogen doped GA (NGA) is a very interesting category of doped GAs due to their mechanical properties [33], lithium storage and transportation rate of Li$^+$ [63]; hence these materials are usually used as electrode materials [64].

In this review, we will be presenting in a systematic way the synthetic strategies pursued for the preparation of GA and will briefly refer to their properties and potential applications. We think that these materials hold great promise in a variety of fields and believe that this review can be useful to both academic and industrial readers.

2. Production methods

Chemically derived GO-based aerogels are the most common 3D graphene structures in the literature [33, 55] because of their facile synthetic route, and the control of pore morphology that they provide. GO has a lot of hydrophobic basal plane and hydrophilic oxygen-containing groups, like hydroxyl, epoxy, carbonyl and carboxyl groups, that facilitate GO to be functionalized through covalent and non-covalent bonding [1, 65–

67]. These basal planes and oxygen-containing groups increase by far the possibility to observe self-assembly of the graphene nanosheets (GNS). It is very important to develop simple and environmental-friendly methods to observe GNS macroassembly, because some other methods that have been reported [6, 68, 69] cannot be exploited for large scale graphene macro-assembly production since they depend on extra chemical reagents and special equipment. Here, the most used and cited routes for producing GAs are divided in four categories; hydrothermal reduction [33], chemical reduction [31], cross-linking [68–72] and template-directed reduction [73, 74] methods. GO is usually produced by chemical oxidation of graphite powder with strong oxidants by employing in most cases the modified Hummers method [75].

2.1. Hydrothermal reduction

The hydrothermal reduction method is the most common and used approach to produce a graphene hydrogel [33], and after drying (either freeze or supercritical), a GA. This method involves the self-assembly of the graphene sheets, as it has been shown that the reduction of GO promotes self-assembly of GNS [33], and finally leads in monoliths and 3D graphene structures. In this method [76–78], conditions of high temperature and high pressure are needed, while the starting solutions are firmly sealed. In that way, the gel rate is controlled and the gel integrality is kept.

During the assembly of GO, chemical reduction and gelation/cross-linking can occur simultaneously. This can be observed in the hydrothermal [33, 79], sol–gel [80] but in other methods, as well [46].

2.2. Chemical reduction

The chemical reduction method uses mild reduction agents like hydrazine, Vitamin C, sodium ascorbate etc [81–84], to restore the sp^2 network [84] as opposed to thermal reduction via high temperature in inert or reducing environment [78], and, is considered to be superior to hydrothermal method, which requires chemical cross-linkers, high temperatures and high pressures [85]. Chemical reduction can be also accomplished using acid [46] or base [86] as the chemical reducing agents. In fact, Zhang *et al* [87] have reported the preparation of 3D graphene assemblies with low density and high porosity from a GO solution that was created with a reaction system of oxalic acid (OA) and sodium iodine (NaI). Also, it has been found that mercaptoacetic acid and mercaptoethanol [88] can be used as reducing agents since they promote *in situ* self-assembling of rGO. The process of chemical reduction of graphene-based materials often leads to a small surface area since the graphene layers restack through a π–π interaction during the process.

The electrochemical reduction is an alternative route to obtain GAs. In general, electrochemical methods are commonly used in the production of

graphene-based materials, and in particular, electrochemical exfoliation of graphite has an exceptional role in the synthesis of graphene of high-quality [89, 90] due to its easy, fast and environmentally friendly character. The graphene sheets can act as substrates for supporting other functional materials, like metal oxides, to create GAs. The use of transition metal oxides into 3D graphene assembly can lead to materials with functionalities [91, 92]. Chen *et al* [93] have proposed a one-step *in situ* electrochemical method to produce graphene/CeO_2 aerogels. Initially, a graphene/CeO_2 colloidal solution was prepared by electrochemical exfoliation of graphite anode and *in situ* deposition of CeO_2 nanoparticles on graphene sheets by mixing electrolyte of $(NH_4)_2SO_4/Ce(NO_3)_3$ and $(NH_4)_2SO_4/(NH_4)_2Ce(NO_3)_6$. Afterwards, the aerogel was produced by freeze-drying. Because of the fact that the standard potential of $Ce^{4+} + e^- \leftrightarrow Ce^{3+}$ is 1.72 V at 298 K, a DC voltage of 10 V can secure the achievement of this redox reaction. Furthermore, OH^- produced by the electrolysis of water and the hydroxyl groups formed on graphene can promote the growth of CeO_2 on the graphene sheets.

2.3. Cross-linking methods

2.3.1. Hydrogen bonds
GO as a hydrophilic compound forms a stable solution in water [94], but this breaks down in strong acidic aqueous media because of the insufficient mutual repulsion [95]. However, if the pH of the GO solution is decreased, the electrostatic repulsion weakens and the hydrogen bonding increases due to the protonation of carboxyls. This leads to the strengthening of the hydrogen bonding and, the formation of a stable GO gelation. Generally speaking, cross-linking agents promote gelation of GO sheets by strengthening the bonding force between the sheets. Common cross-linkers are hydroxyl [70], oxygen-containing [94] or nitrogen functional groups [96].

2.3.2. Multi-valent metal ions
It has been found that the self-assembly and gelation of GO sheets is promoted by divalent and trivalent ions like Ca^{2+}, Mg^{2+}, Pb^{2+}, Cr^{3+} [94, 97] and other. These metal ions interact with single GO by a bonding force. The concentration of GO affects the pore density and size.

The sol–gel method is another strategy to develop GAs. In this method, the bonding between GO sheets is stronger than the cross-linking method, because polymerization creates covalent bonds between the sheets [72]. Meng *et al* [44] have reported that alkali-treated GO (AGO) acts as solid base catalyst to initiate the polymerization of resorcinol with formaldehyde (figure 1), which by pyrolization turns into graphene. The graphene/carbon aerogels that were synthesized can be used in supercapacitors because of their specific capacitance (122 F g^{-1} at a constant current density 50 mA g^{-1}). The final composite graphene/carbon aerogels show large surface area (361–763 m^2 g^{-1}), low density (0.11–0.19 g cm^{-3}), high pore volume, narrow pore size distribution (10–50 nm) and high conductivity (528 S m^{-1}).
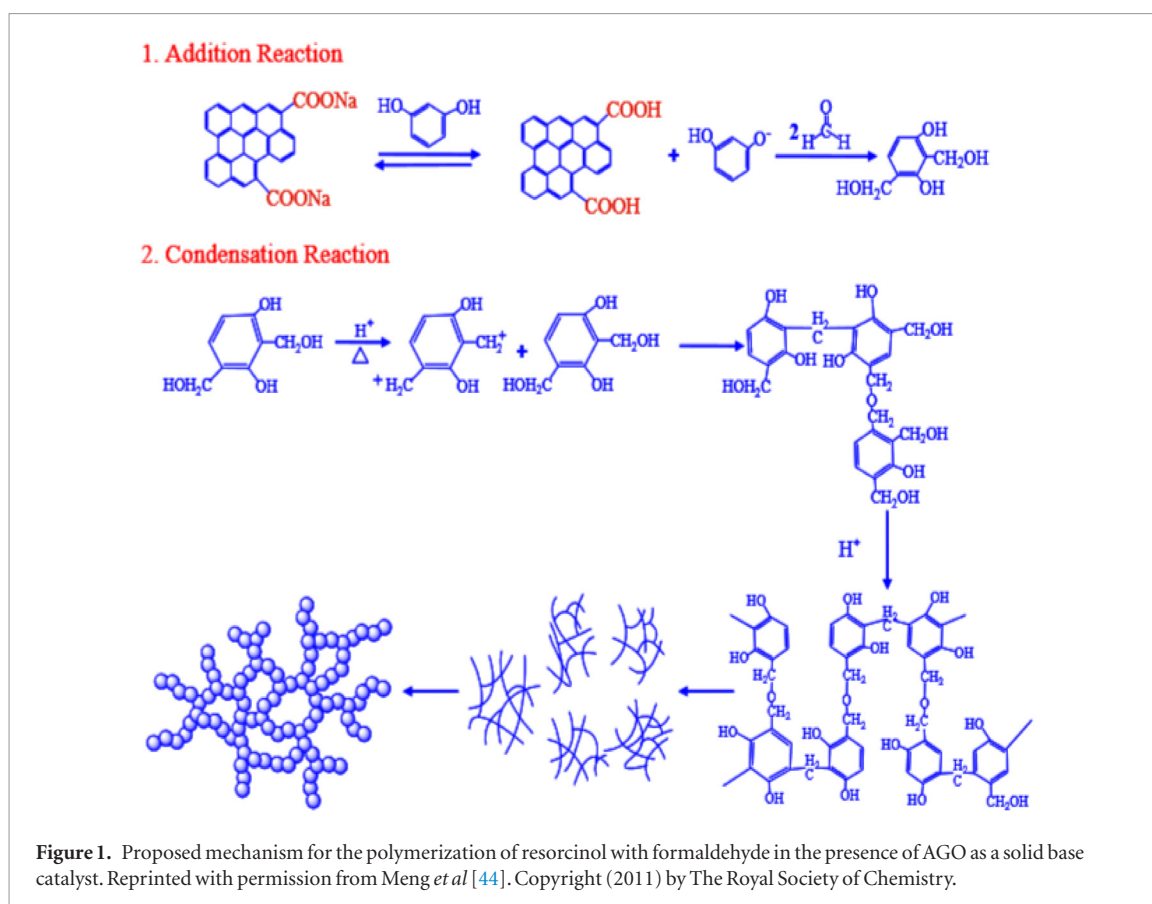
2.4. Template-directed reduction
Template-directed reduction is a very useful method for obtaining porous GAs [98] because it prevents random interconnection structures while it favours controllable and uniform macropores and tailorable microstructure as well. Chen *et al* [73] have reported the synthesis of a macroporous 'bubble' graphene film through a template-directed reduction method. Some latex spheres of monodisperse polymethyl methacrylate (PMMA) acted as the hard templates in this material. A GO hydrosol and a PMMA spheres suspension were mixed, and after filtration, a composite film was extracted and calcinated at 800 °C leading to the PMMA template and to thermally reduced GO into graphene at the same time. From the thermogravimetric results, it was found that the oxygen-containing functional groups of GO are removed at 230 °C, while the PMMA spheres are pyrolyzed and removed at 400 °C. Graphene was finally derived with the PMMA spheres acting as the interlayer spacer. The synthesized material exhibited high electrochemical capacitance. A similar method is ice template-directed method [74] that takes advantage of the freeze drying approach. Porous GAs in aqueous solutions [6, 99] can be produced with this method, while meso- and macro-porosity can be controlled through dipping rate and freezing temperature.

2.5. Recent progresses on GAs synthesis

2.5.1. 3D printing-freeze drying
Lin *et al* [100] presented a freeze gelation (RTFG) method at RT to prepare pristine graphene (PG) aerogels starting from exfoliated material (PG, and, both rGO and rGO solutions). This method is very close to aqueous freeze gelation but here the water is substituted by an organic solvent with a boiling point higher than RT and high vapour pressure. In RTFG, the starting material is mixed with the solvent above its boiling point, usually for temperatures between 50 and 120 °C, and cooled to form a solid state material at RT. The solvent should have a higher vapour pressure than the solid at RT and ambient pressure conditions in order to obtain rapid sublimation which yields a solid material with high porosity [101–103]. The advantages of this method over aqueous freeze gelation is, firstly, that the solid is formed through conventional processing methods prior to sublimation, while with aqueous methods freezing takes place strictly in a container, and secondly, the plurality of solvents that can be used which allow materials to be dispersed without functionalization agents or surfactants.

In figure 2(a), there is an illustration of RTFG application for GAs. At first, PG flakes are soluted to the desired concentration in a solvent at high temperature, with sonication. Then, the solution is treated with the

Figure 1. Proposed mechanism for the polymerization of resorcinol with formaldehyde in the presence of AGO as a solid base catalyst. Reprinted with permission from Meng *et al* [44]. Copyright (2011) by The Royal Society of Chemistry.

appropriate forming process such as moulding, extrusion or printing and cooled to be solidified. The solvent is evaporated at RT leaving behind a nanostructured porous GA.

3D printing has also been exploited to prepare GO aerogels with complex shapes [104–106]. In these cases, an aqueous solution of GO is formed in a polymer solution to promote gelation after deposition. Gelation is achieved through water removal either by freeze drying or supercritical drying. Subsequently, an rGO aerogel is formed by reduction at elevated temperatures. The RTFG method can also be used with starting materials mixtures of rGO and multiwalled carbon nanotubes (MWCNTs), mixtures of graphene flakes and MWCNTs, while the polymers addition in these mixtures enhances the strength of the final aerogel. The microstructure of the final product depends on the graphene concentration, the solvents employed, the concentration of the polymer in the solution and the cooling rate. In figures 2(b) and (c), the microstructure of PG aerogels is shown. Solute rejection during solidification leads to solvent rich regions, that create a microporosity of relatively large voids after evaporation, and graphene rich regions that lead to a structure containing random packing of the PG flakes leading to nanoporosity within the microporous structure walls. As shown in figure 2(b), the aerogel with phenol has a characteristic lamellar structure which is very close to the corresponding microstructures formed with conventional aqueous freeze casting [107]. In contrast,

the aerogel formed using camphene shows an equiaxed microstructure with no directionality.

The mechanical properties of the PG aerogels are shown in figure 3. The PG aerogels with graphene concentration of 20 and 40 mg cm^{-3} had Young's modulus values equal to 7.7 ± 1.0 and 82.5 ± 4.0 kPa, respectively, and yield strength of 0.4 ± 0.01 and 2.1 ± 0.2 kPa (figure 3(c)). With the addition of poly(vinyl alcohol) (PVA) in the solution with the phenol, the Young's modulus of the aerogels increased to 553 ± 85 and 893 ± 82 kPa for the same concentrations of 20 and 40 mg cm^{-3}, respectively, and yield strengths of 25 ± 2 and 51 ± 3 kPa (figure 3(d)).

The Raman spectra of the PG flakes and the aerogel produced using phenol are shown in figure 4(a). The 2D peak shifts from 2666 cm^{-1} for PG to 2656 cm^{-1} for the aerogel, while the 2D:G peak intensity ratio increases from 0.4 to 0.63. The observed shift and the increase of the 2D peak intensity indicate that the graphene in the aerogel is of higher quality than the PG, noting that the PG may be further exfoliated during mixing. This is indicative of the presence of high quality few layer graphene sheets in the aerogel, without flake restacking and aggregation during processing. Gas adsorption was used to find the mean specific surface area of the aerogels (figures 4(b) and (c)). A small amount of MWCNTs that was added to the PG solution (20 wt.% MWCNTs) affects significantly the aerogel microstructure and the physical properties, like density (to 6.5 mg cm^{-3} from 2.5 mg cm^{-3}). The PG and PG/MWCNTs
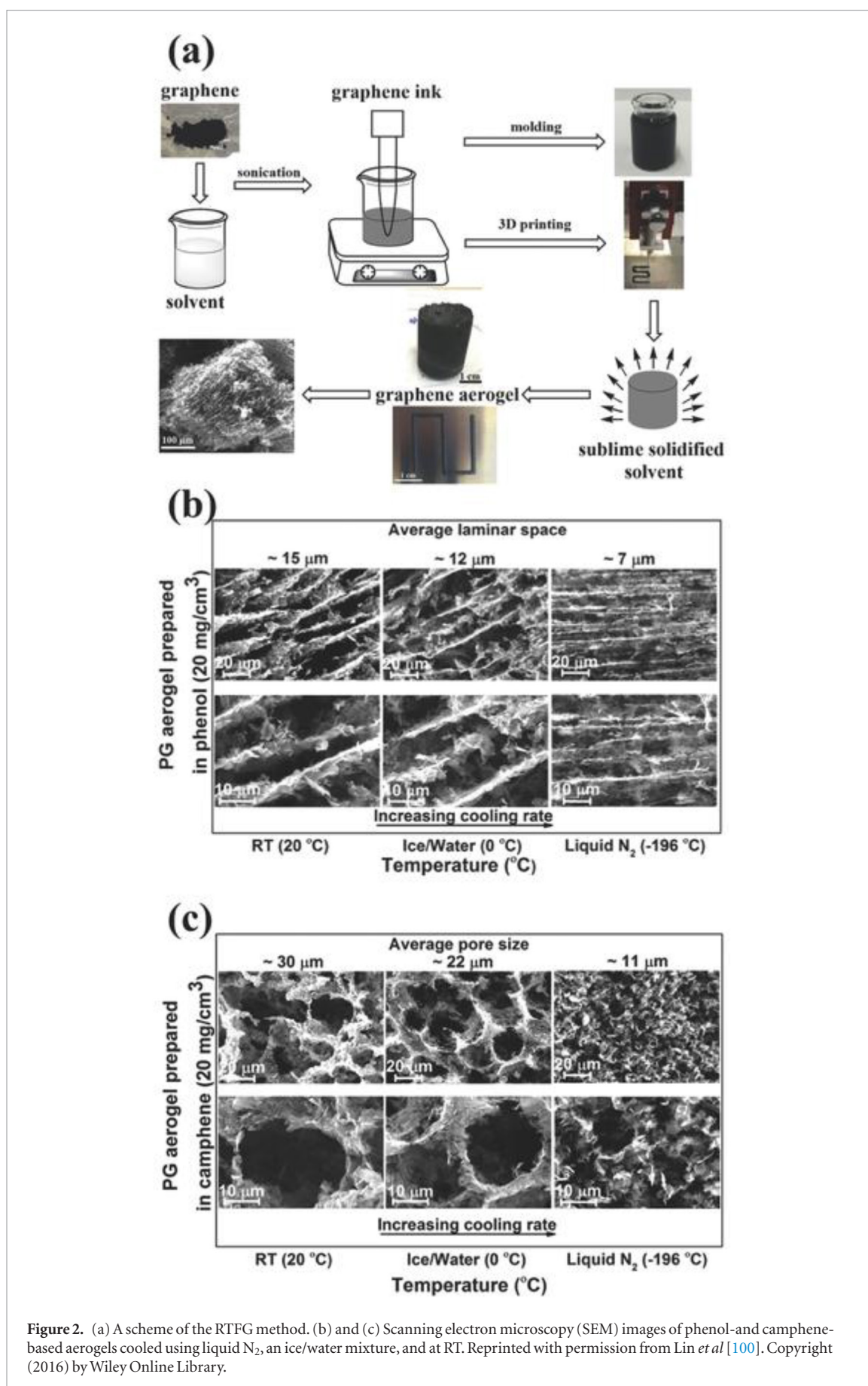
Figure 2. (a) A scheme of the RTFG method. (b) and (c) Scanning electron microscopy (SEM) images of phenol-and camphene-based aerogels cooled using liquid N$_2$, an ice/water mixture, and at RT. Reprinted with permission from Lin *et al* [100]. Copyright (2016) by Wiley Online Library.

aerogels show specific surface areas of approximately 400 and 700 m^2 g^{-1}, respectively (figure 4(c)). These values can be compared to those from GAs produced by other methods [104, 108]. The pore-size distribution lies of the 10–200 nm range has a peak pore diameter at 73 nm for the PG aerogel and 83 nm for the PG/MWC-NTs aerogel (figure 4(c)). The electrical conductivity of the PG aerogel as a function of density (figure 4(d))
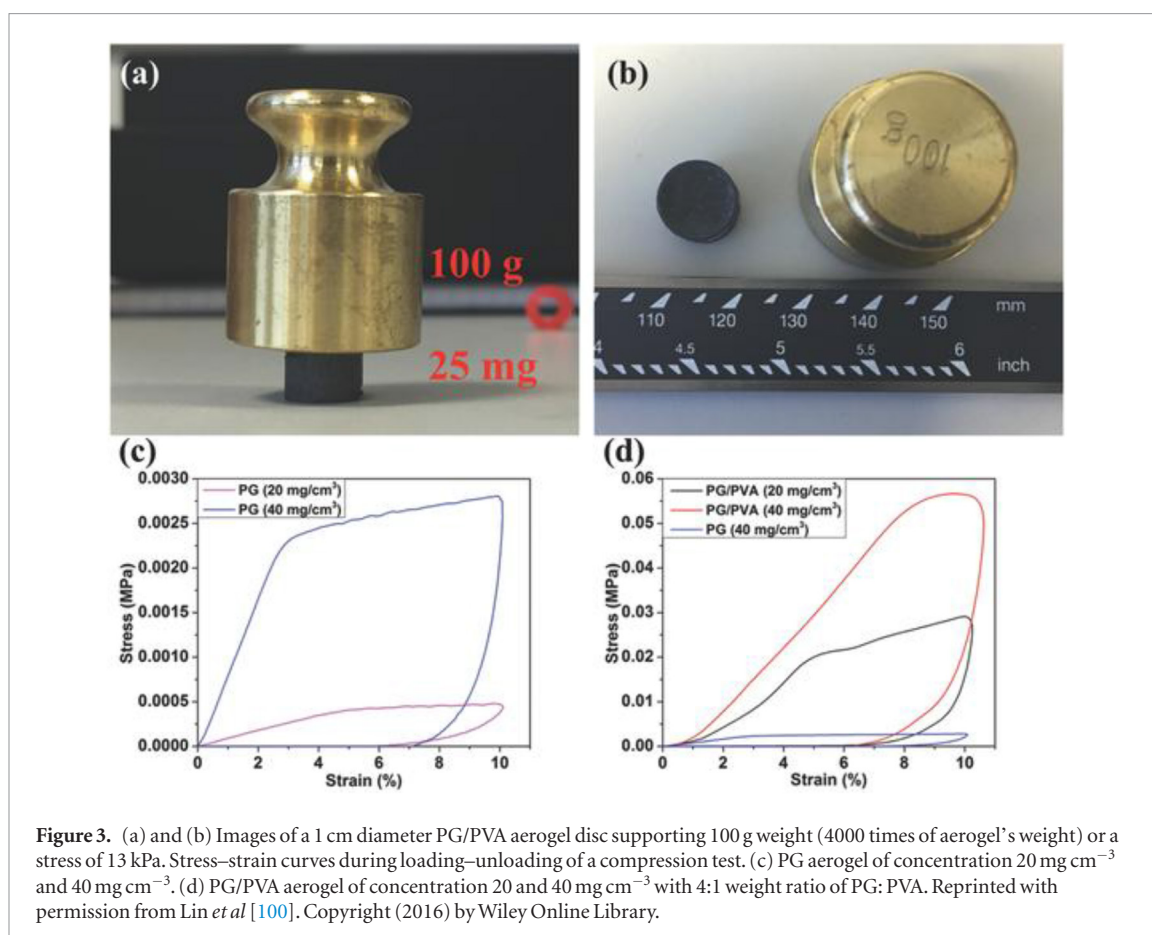
Figure 3. (a) and (b) Images of a 1 cm diameter PG/PVA aerogel disc supporting 100 g weight (4000 times of aerogel's weight) or a stress of 13 kPa. Stress–strain curves during loading–unloading of a compression test. (c) PG aerogel of concentration 20 mg cm^{-3} and 40 mg cm^{-3}. (d) PG/PVA aerogel of concentration 20 and 40 mg cm^{-3} with 4:1 weight ratio of PG: PVA. Reprinted with permission from Lin *et al* [100]. Copyright (2016) by Wiley Online Library.

shows a maximum value of 9 S cm^{-1} at a density value of 20 mg cm^{-3}. Although this value is slightly lower than those produced by CVD onto sacrificial templates [56], it is higher than those of rGO-based aerogels [109] and CNT foams [72].

The synthesized aerogels show high specific capacitance, very good electrochemical stability and a high reversibility. These aerogels can be used as electrodes in supercapacitors. Attention should be paid to the choice of solvent as it affects the microporous structure.

Zhu *et al* [106] reported a method of direct ink writing for fabricating GAs. This is done via a 3D printing technique known as direct ink writing. This technique uses a three-axis motion to create 3D structures by mechanically extorting a continuous ink filament through a micronozzle at RT and depositing it layer-by-layer [110]. The 3D printing technique is a very convenient method for fabricating several aerogel architectures which can be applied to different fields. The so-made GAs are lightweight, exhibit high conductivity and remarkable supercompressibility (up to 90% compressive strain). Also, the Young's moduli of the aerogels ($\approx$25 MPa) appear to be higher than those of other bulk graphene aerogels ($\approx$2.5 MPa).

The stability of the cyclic resilience of printed GAs and the compression cycling of the GA at 50% strain are shown in figures 5(a) and (b). As seen, the energy loss coefficient of printed aerogels decreases from 60 to 30% in the first three cycles and then remains constant. The highest stress for each cycle in figure 5(a) also shows a

similar behaviour (figure 5(b)). The electrical resistance of the printed GAs is also shown versus cyclic compression (figure 5(c)). We can notice a small decrease after multiple compressions, confirming the high structural resilience of the GA microlattices. The Young's modulus, *E*, as a function of density for the printed GAs and standard GAs (bulk) vis-à-vis values obtained from other carbon, carbon nanotube and graphene assemblies reported in the literature [46, 86, 109, 111–115] are shown in figure 5(d). In fact, the bulk aerogel data are close to literature data, while the printed aerogel data are clearly off the known curve. For both cases, Young's modulus, *E,* was found to scale linearly with density, $\rho^{2.5}$. The similar values of the exponent ($\approx$2.5) suggest that both printed and bulk aerogels have the same bending behaviour under compression. But, for the graphene microlattices *E* is about one order of magnitude larger than that of most bulk GAs for the same densities. So, the printed GAs can exhibit higher stiffness with much lower density compared to higher density bulk aerogels.

The real challenge for this fabrication is the development of printable GO inks with appropriate composition and rheology. Nevertheless, this proposed method is very promising and the GA structures of desired shapes can lead to new energy storage devices, graphene-based electronics, separation devices and catalytic scaffolds.

Very recently, Scaffaro *et al* [116] reported the synthesis of an ultralight graphene oxide-polyethylene glycol aerogel (GPA) with some attractive characteristics
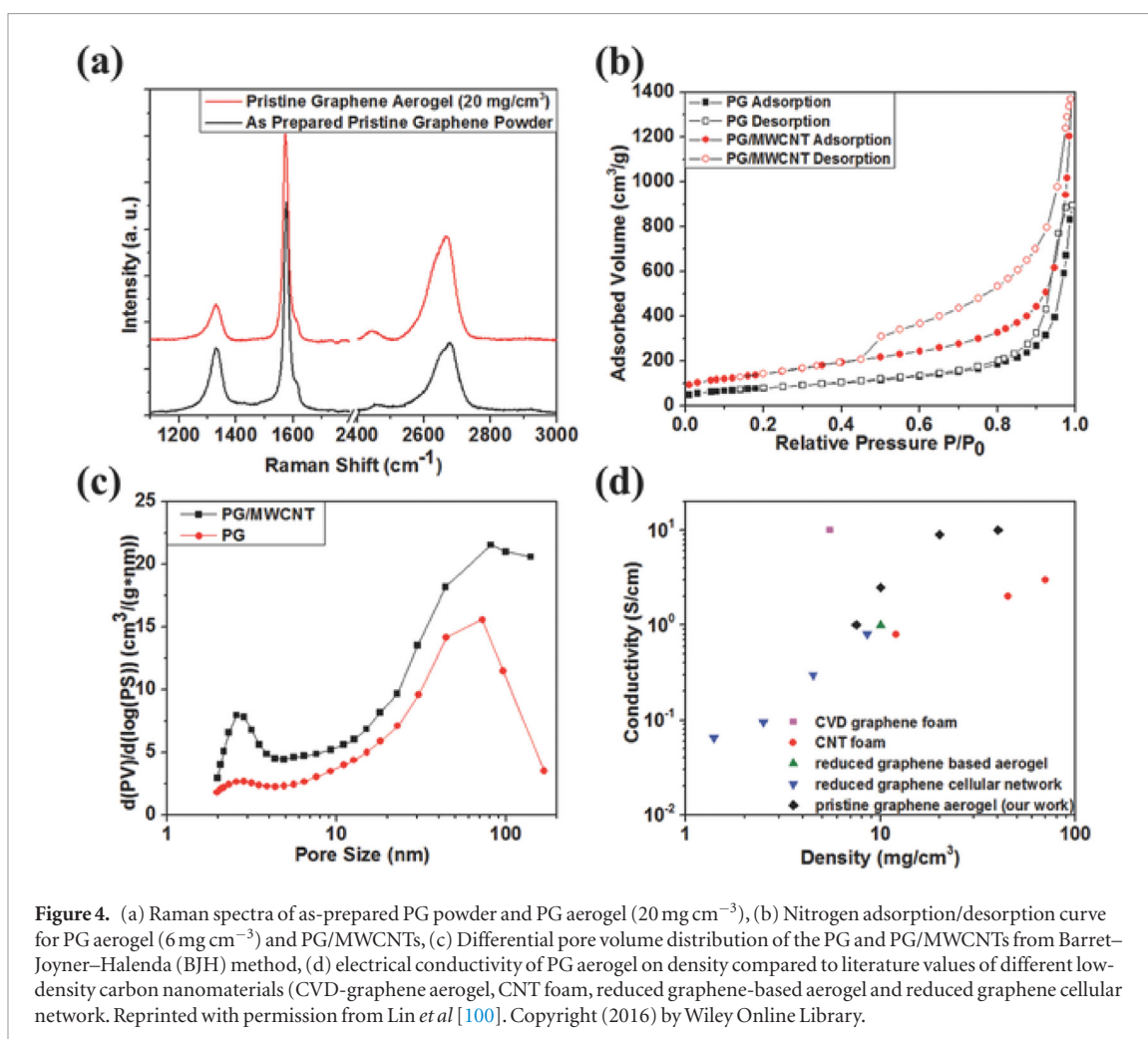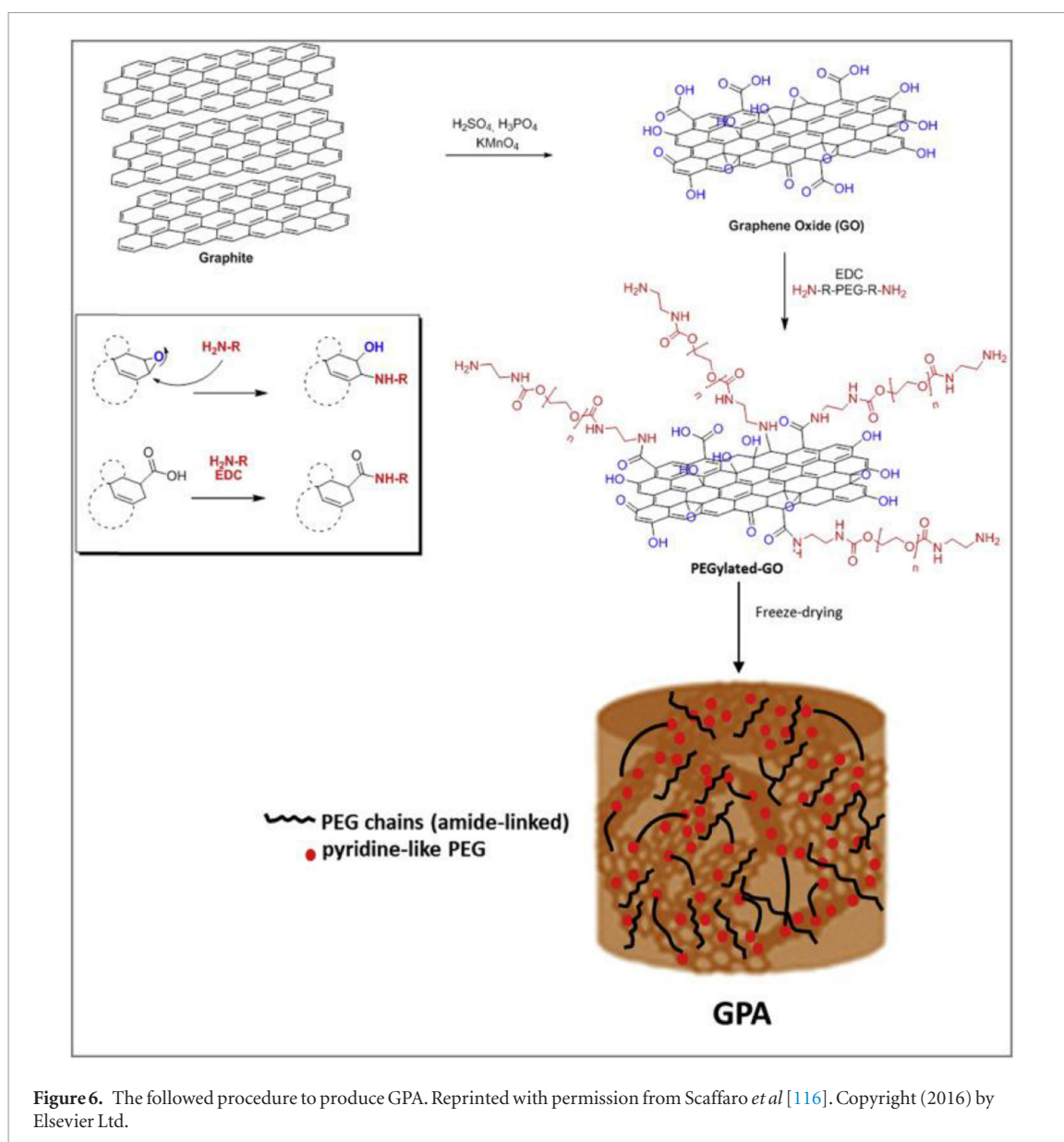
Figure 4. (a) Raman spectra of as-prepared PG powder and PG aerogel (20 mg cm^{-3}), (b) Nitrogen adsorption/desorption curve for PG aerogel (6 mg cm^{-3}) and PG/MWCNTs, (c) Differential pore volume distribution of the PG and PG/MWCNTs from Barret–Joyner–Halenda (BJH) method, (d) electrical conductivity of PG aerogel on density compared to literature values of different low-density carbon nanomaterials (CVD-graphene aerogel, CNT foam, reduced graphene-based aerogel and reduced graphene cellular network. Reprinted with permission from Lin *et al* [100]. Copyright (2016) by Wiley Online Library.
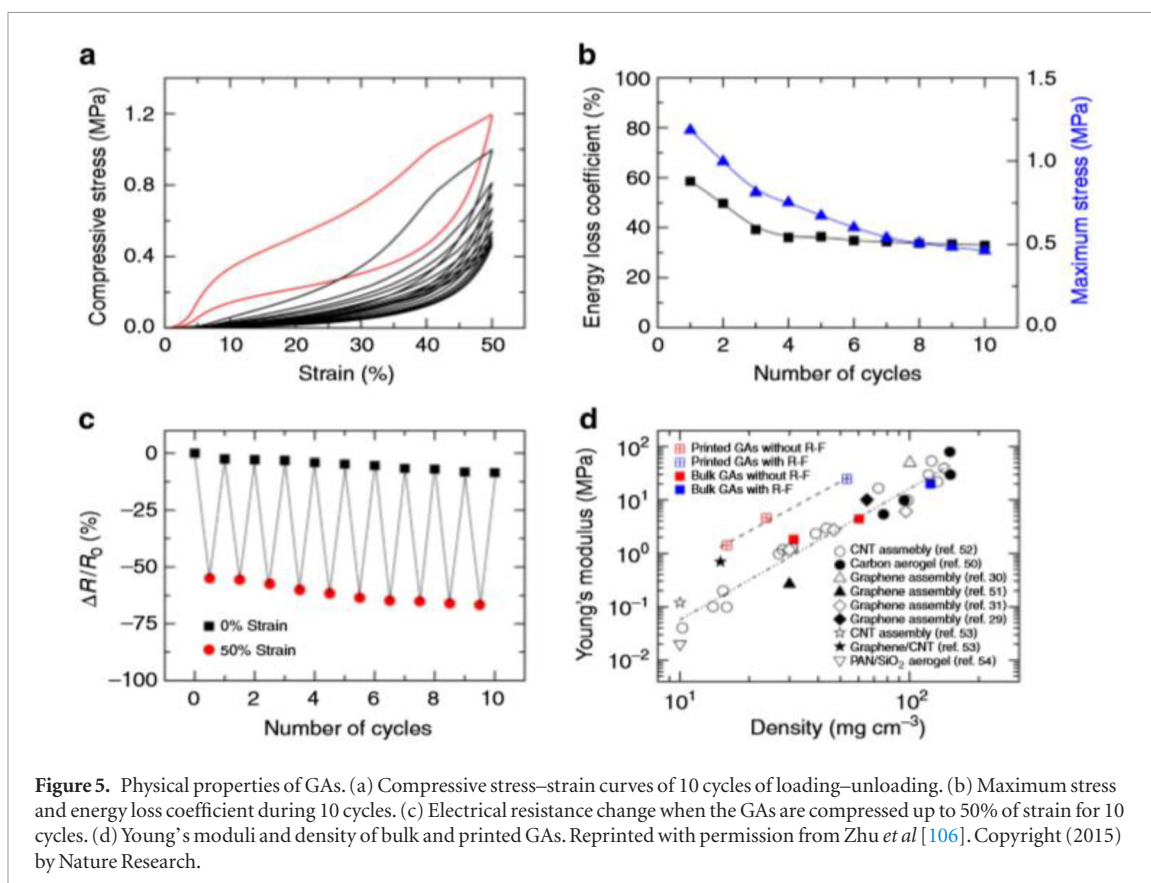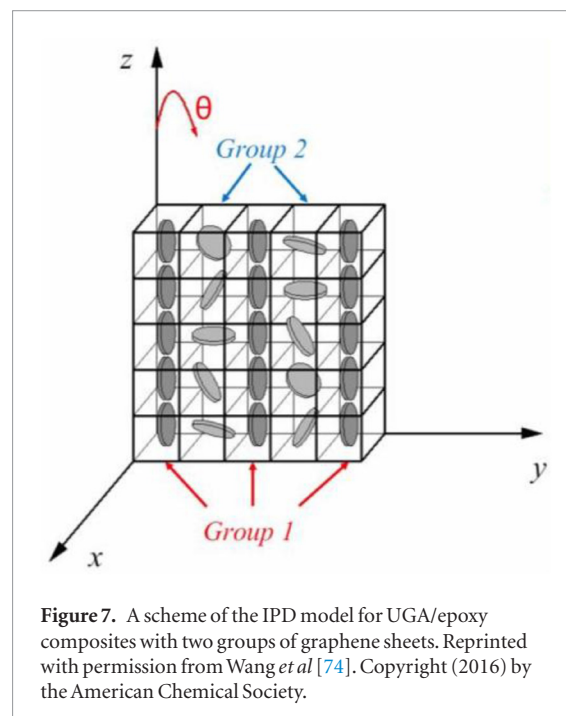

Figure 5. Physical properties of GAs. (a) Compressive stress–strain curves of 10 cycles of loading–unloading. (b) Maximum stress and energy loss coefficient during 10 cycles. (c) Electrical resistance change when the GAs are compressed up to 50% of strain for 10 cycles. (d) Young's moduli and density of bulk and printed GAs. Reprinted with permission from Zhu *et al* [106]. Copyright (2015) by Nature Research.

Figure 6. The followed procedure to produce GPA. Reprinted with permission from Scaffaro *et al* [116]. Copyright (2016) by Elsevier Ltd.
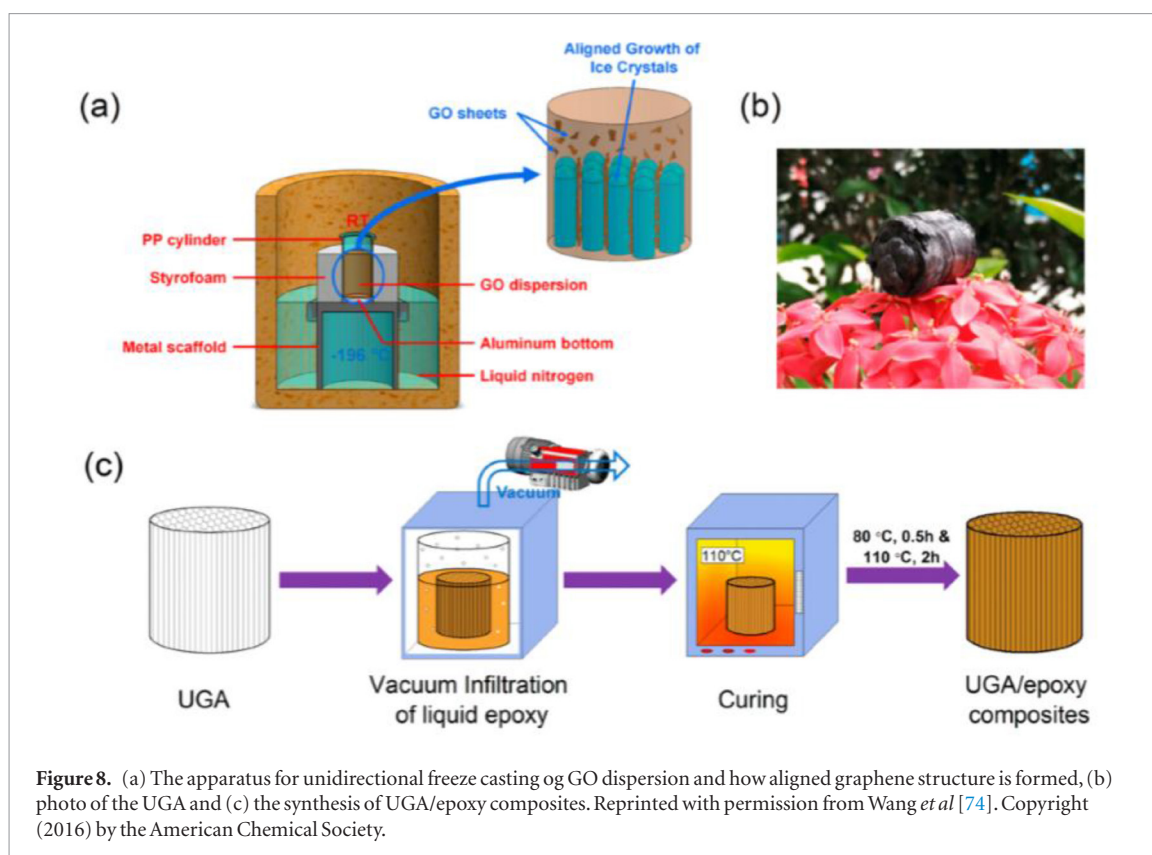
such as high porosity, high surface area, biocompatibility, cytocompatibility and outstanding mechanical behaviour. As shown in figure 6, firstly, GO is coupled with an amino-terminated polyethylene glycol (PEG-NH$_2$) sample using carbodiimide (EDC). The coupling approves the creation of covalent bonds between –NH$_2$ functional group of the polymer and the epoxy and carboxyl groups of GO. Afterwards, the hydrogel is converted into aerogel by freeze-drying.

Wang *et al* [74] have reported the fabrication of GAs with a highly aligned porous structure, ultralow densities, large surface areas and excellent electrical conductivities. This fabrication was accomplished through a novel unidirectional freeze casting method. The highly orientated graphene sheets resulted from the expulsion of GO sheets by the rapidly advancing ice fronts that forced them to be placed between the aligned ice crystals, as shown in figure 8(a). The final unidirectional GA (UGA, figure 8(b)) was converted by vacuum-assisted infiltration into of liquid epoxy UGA/epoxy composites. These composite materials show a very low perco-

Figure 7. A scheme of the IPD model for UGA/epoxy composites with two groups of graphene sheets. Reprinted with permission from Wang *et al* [74]. Copyright (2016) by the American Chemical Society.

Figure 8. (a) The apparatus for unidirectional freeze casting og GO dispersion and how aligned graphene structure is formed, (b) photo of the UGA and (c) the synthesis of UGA/epoxy composites. Reprinted with permission from Wang *et al* [74]. Copyright (2016) by the American Chemical Society.

lation threshold of 0.007 vol.% because of the highly aligned, 3D interconnected conductive networks of UGA. An analytical model was developed based on the average interparticle distance (IPD) theory [117] to simulate the percolation behaviour and define the percolation threshold of these UGA/epoxy composites. According to the model, V_c, which is the required volume fraction for single type fillers with several shapes to form conductive networks, is given by:

$$V_c = \frac{\pi}{4}\left(\frac{1}{R}\right) \qquad (1)$$

where R is the percolation factor which depends on the size, shape and the orientation state of the fillers in the composite materials. For 2D disc-shaped fillers like graphene, the percolation factor, R_S, is given by:

$$R_S \approx \left(\frac{D}{t}\right)\langle\cos^2\theta\rangle^3 \qquad (2)$$

where D and t are the diameter and thickness of graphene, respectively, and $\cos^2\theta$ is the average orientation angle between the fillers and the direction of preferred orientation. In the IPD model, it is assumed that the composite is divided into cubic elements, each containing one filler in the centre, and the percolation occurs when the unit volume is filled with single type of cubic elements. Similarly, for composites containing two different groups of fillers, we may assume that the percolation occurs when the unit volume is filled with two groups of cubic cells, as shown in figure 7.

The unidirectional freeze casting method is illustrated in figure 8(a). GO dispersions with different concentrations are poured into a propylene (PP) con-

tainer with a conductive aluminum bottom for thermal exchange with the underlying liquid nitrogen. The PP container is insulated with styrofoam and mounted on the top of a metal scaffold. The container along with the scaffold is rested in a pool of liquid nitrogen with the same depth. Then, a large temperature gradient is applied between the bottom ($-196\,°C$) and the top (RT) of the GO dispersions and so, the ice crystals grow along a vertical direction. After freeze drying of the freeze-cast dispersion, a GO aerogel is formed. This aerogel is reduced to UGA by controlled heat treatment. The UGA/epoxy composition is illustrated in figure 8(c). Epoxy resin, curing agent and acetone are mixed with specific weight ratio. This mixture is mounted in a vacuum oven to sublime acetone at RT, and then is heated to $60\,°C$ to lower the viscosity of resin. Then, the mixture is poured into the UGA, followed by infiltration under vacuum and curing. Nevertheless, the UGAs that were produced with low concentration of GO (e.g. $0.5\,mg\,ml^{-1}$) did not exhibit a similar behaviour. Loosely interconnected graphene sheets with little alignment were observed and also the GO sheets were not close to each other in the dispersion.

Wei *et al* [118] have prepared Ni-doped graphene/carbon cryogels (NGCCs) by adding R and F to a GO suspension, using Ni^{2+} as catalysts for the gelation. The Ni^{2+} enrich the crosslinking between GO and RF skeletons, strengthening the cryogel. The starting hydrogel is converted to aerogel through freeze-drying and subsequent carbonization under an inert atmosphere. After this phase, 3D interconnected structures are observed that enhance the mechanical properties. Ni^{2+} are converted into Ni nanoparticles during car-
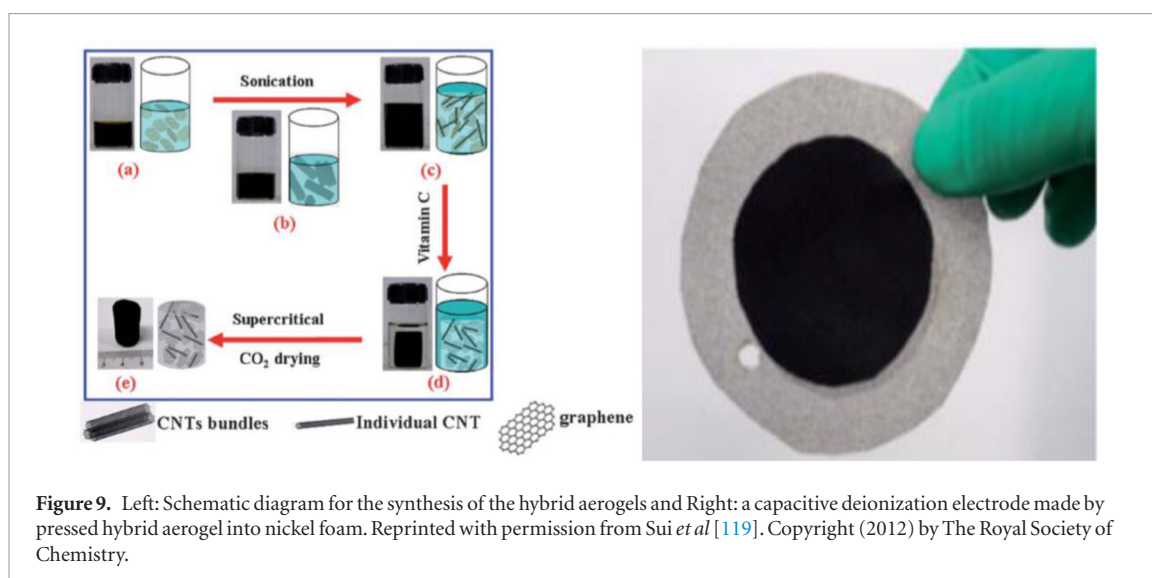
Figure 9. Left: Schematic diagram for the synthesis of the hybrid aerogels and Right: a capacitive deionization electrode made by pressed hybrid aerogel into nickel foam. Reprinted with permission from Sui *et al* [119]. Copyright (2012) by The Royal Society of Chemistry.
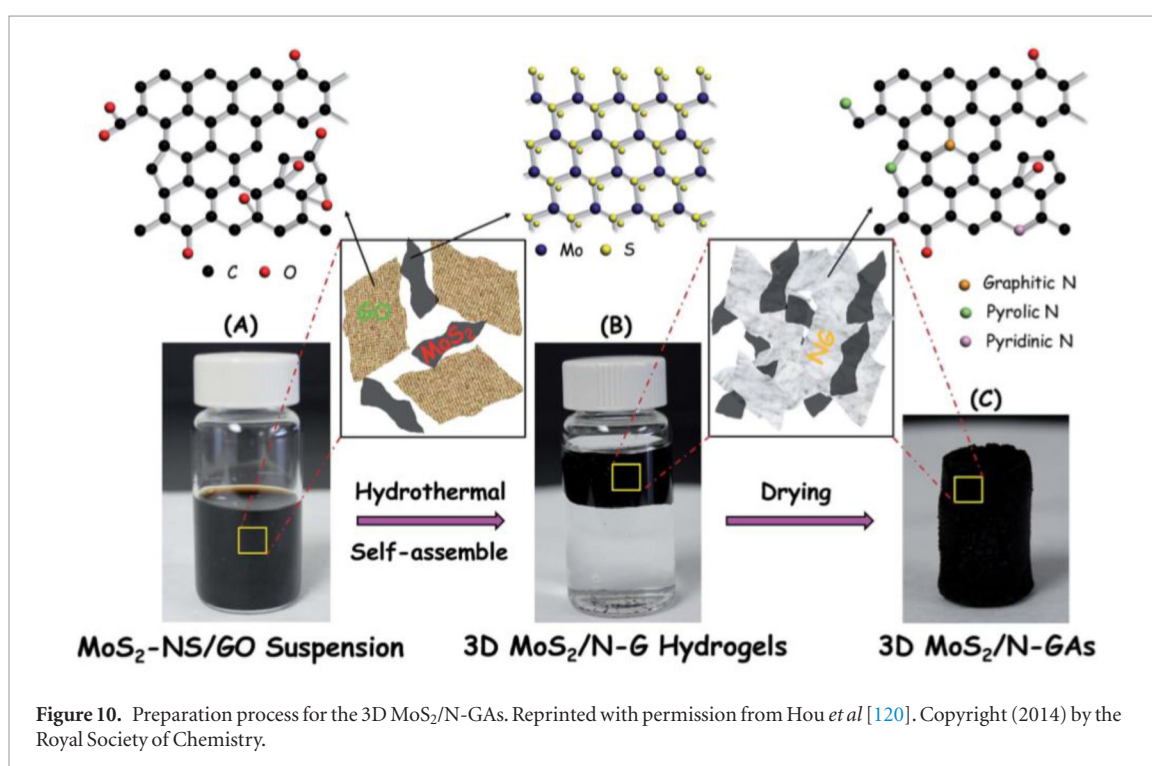
Figure 10. Preparation process for the 3D MoS$_2$/N-GAs. Reprinted with permission from Hou *et al* [120]. Copyright (2014) by the Royal Society of Chemistry.

bonization, and consequently, they are incorporated in the interconnected structures. The NGCCs can be applied in water purification since their porosity within the interconnected structures enables them to absorb oils and some organic solvents, while it can be recycled as a bulk material.

2.5.2. Chemical reduction-hydrothermal process

Sui *et al* [119] have fabricated hybrid aerogels of carbon nanotubes (CNTs)-graphene via supercritical CO$_2$ drying after heating aqueous suspensions of GO and CNTs with Vitamin C. Figure 9 shows a schematic diagram for the synthesis of the hybrid aerogels (on the left) and a photo of a capacitive deionization electrode made by pressed hybrid aerogel into nickel foam (on the right). These hybrid aerogels can be applied in water purification since they can deionize light metal salts,

remove organic dyes and enrich heavy metal ions like Pb^{2+}, Ag$^+$, etc. They exhibit high conductivity of 7.5 S m^{-1}, large surface area of 435 m^2 g^{-1}, pore volume of 2.58 cm^3 g^{-1} and maximum desalination capacity of 633.3 mg g^{-1}. Nevertheless, supercritical CO$_2$ drying has a negative environmental impact, so the claimed by the authors 'green' synthesis is not fully convincing.

Hou *et al* [120] have reported the preparation of a 3D hybrid of layered MoS$_2$/nitrogen-doped graphene nanosheet aerogels (3D MoS$_2$/N-GAs) by a hydrothermal process. Their intention was to examine the possible application of the aerogel as a novel catalyst for hydrogen production from organic wastes and particularly from microbial electrolysis cells (MECs). A high output current density of 0.36 mA cm^{-2} with a hydrogen production rate equal to 0.19 m^3 H$_2$/m^3 · d was observed for the material at 0.9 V bias. Figure 10

describes the preparation process for the 3D MoS$_2$/N-GAs. At the beginning, MoS$_2$/NS was produced by liquid exfoliation method using MoS$_2$ as the source material. Then, the MoS$_2$/NS was mixed with GO and ammonia solutions and afterwards this mixture was assembled hydrothermally to form a 3D MoS$_2$/N-GA. Following this process, the MoS$_2$/NS was deposited on graphene nanosheets with the simultaneous reduction of GO and the enhancement of nitrogen particles into the graphene network.

Zhang *et al* [77] have presented a synthesis of 3D porous hybrids consisted of ultrathin defect-rich MoS$_2$ nanosheets (dr-MoS$_2$ NSs) and conductive graphene nanosheets (GNS) through hydrothermal co-assembly procedure. Firstly, the ultrathin dr-MoS$_2$ NSs are dispersed in aqueous solution, and then, are mixed with GO to co-assemble into 3D porous dr-MoS$_2$ NSs structures. The mixed dispersion, after sealing it tightly into a Teflon-lined stainless steel autoclave, is heated at 180 °C for 12 h. Finally, the thermal reduction of GO to GNS, takes place at 800 °C for 2 h in N$_2$ atmosphere. These synthesized hybrids show a large specific surface area that facilitates rapid diffusion of Li$^+$ to access active materials. The dr-MoS$_2$ NSs, due to their additional active edge sites, are responsible for the intercalation of Li$^+$ that results in higher specific capacity. The interconnected graphene network contributes to higher conductivity (better charge transfer and Li$^+$ transport), while it secures the material's stability during lithiation/delithiation. So, these materials exhibit an excellent electrochemical performance (reversible capacity of 1130.9 mA · h g^{-1} at a current density of 0.1 A g^{-1}), something that is ascribed to their 3D porous structure and the synergetic effect between ultrathin dr-MoS$_2$ NSs and conductive graphene network. Consequently, some new promising anode materials can be based on these structures. In table 1, GAs produced by different approaches and methods are listed.

2.5.3. Other methods

A novel procedure to fabricate graphene/carbon aerogels with multimodal pores (from micropores to mesopores and macropores) via carbonization of graphene crosslinked polyimide (PI) aerogels, was reported by Zhang *et al* [121]. At first, GO-poly (amic acid) (PAA, polyimide precursor) aerogels were synthesized by mixing PAA and a GO suspension. Then, the as-synthesized aerogels were amidated in nitrogen atmosphere under 100, 200 and 300 °C for 1 h in order to crosslink PAA with GO and GO to be reduced to graphene. At the last stage, graphene/carbon aerogels are observed by carbonization of graphene crosslinked PI aerogels. Graphene seems to have a powerful crosslinking action which accelerates the gelation process, improves the porous structures inside carbon aerogels (reducing the pore size while increasing the amount of micro- and meso-pores), and increases the specific surface area and conductivity of the aerogels (forming a 3D conductive network). With

graphene incorporation, these aerogels show a specific surface area of 998.7 m^2 g^{-1} and specific capacitance of 178.1 F g^{-1} at a current density of 1 A g^{-1}, instead of the respective values for pure carbon aerogels (193.6 m^2 g^{-1} and 104.2 F g^{-1}). The dual interest of this process is that it produces high performance of carbon aerogels with hierarchical structures while broadens the applications of polyimide.

Also, some PI composite aerogels with enhanced flame-retardant property have been produced after the addition of friendly flame-retardant additives, like graphene and montmorillonite (MMT) through freeze-drying and followed by thermal imidization method [122]. The GO/MMT hybrid, is well dispersed in PI matrix due to the strong interaction between the two materials and that improves the mechanical, thermal and flame-retardant properties of the aerogels. For the composite aerogels, compression modulus has been found to be equal to 14 MPa, specific modulus equal to 155.5 MPa · cm^3 g^{-1}, while 574.3 °C were needed to decompose 10% of the weight of these PI/graphene/MMT aerogels, a value that is 20 °C higher than that of pure PI aerogels. Last but not least, the composite aerogels increased the limiting oxygen index (LOI) up to 55. A high LOI is equivalent to a better flame-retardant performance.
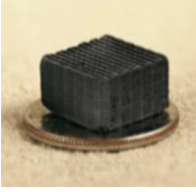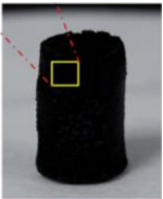
3. Applications

As mentioned above, the GAs can be produced by different methods and that leads to materials with enhanced properties such as high electrical conductivity, high mechanical strength, thermal stability and high adsorption capacity for dyes, oils, organic solvents and inorganic ions. Thus the GAs can be exploited in a whole range of applications such as electrodes for electrochemical power sources and LIBs, as supercapacitors, in air purification, in removal of several oils and dyes from water and generally in waste water management, as discussed below.

3.1. Energy storage

Zhang *et al* [46] reported the preparation of mechanically strong and electrically conductive GAs. The starting material was GO that was reduced with L-ascorbic acid and the aerogels can be synthesized by either freeze drying or supercritical drying. The GAs exhibit a specific capacitance of 128 F g^{-1} and could be used as electrodes for electrochemical power sources. Also, it is remarkable that the aerogel can stand 14 000 times its own weight, which is twice the value exhibited by carbon nanotubes [124]. Qiu *et al* [125] have reported the synthesis of TiO$_2$/GA composite materials. These materials were studied as electrodes for lithium-ion batteries (LIBs) and solar light photocatalysts. The reason behind this is that GAs are able to facilitate multidimensional electron transport and adsorb organic pollutants. The used method was one step hydrothermal method through which *in situ*

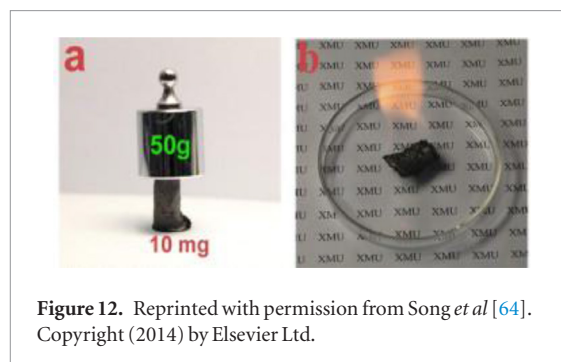**Table 1.** Concentrating table for GAs synthesized with different techniques.

GA name	Synthesis method	Properties	Photo	Reference
Graphene/ carbon aerogels	Sol–gel	Specific capacitance of 122 F g^{-1} at a constant current density 50 mA g^{-1}, surface area of 361–763 m^2 g^{-1}, density of 0.11–0.19 g cm^{-3}, high pore volume, narrow pore size distribution (10–50 nm) and high conductivity.		Reprinted with permission from Meng F, Zhang X, Xu B, Yue S, Guo H and Luo Y 2011 Alkali-treated graphene oxide as a solid base catalyst: synthesis and electrochemical capacitance of graphene/carbon composite aerogels *J. Materi. Chem.* **21** 18537. Copyright (2011) by The Royal Society of Chemistry.	[44]
PG aerogels	Room temperature freeze gelation (RTFG)- freeze or supercritical drying	High specific capacitance, good electrochemical stability and high reversibility		Reprinted with permission from Lin Y, Liu F, Casano G, Bhavsar R, Kinlock I A and Derby B 2016 Pristine graphene aerogels by room-temperature freeze gelation *Adv. Mater.* **28** 7993. Copyright (2016) by Wiley Online Library.	[100]
GPA	Polymerization-freeze drying	High porosity, specific surface area, biocompatibility, cytocompatibility, good mechanical properties		Reprinted with permission from Scaffaro R, Maio A, Lopresti F, Giallombardo D, Botta L, Bondi M L and Agnello S 2016 Synthesis and self-assembly of a PEGylated-graphene aerogel *Compos. Sci. Technol.* **128** 193. Copyright (2016) by Elsevier Ltd.	[116]
UGA	Freeze casting-freeze drying	Highly aligned porous structure, ultralow densities, large surface areas and excellent electrical conductivities	—	[123]
GA microlattices	Direct ink writing	Light weight, high conductivity and remarkable supercompressibility: up to 90% compressive strain		Reprinted with permission from Zhu C, Han T Y-J, Duoss E B, Golobic A M, Kuntz J D, Spadaccini C M and Worsley M A 2015 Highly compressible 3D periodic graphene aerogel microlattices *Nat. Commun.* **6** 6962. Copyright (2015) by Nature Research.	[106]
Hybrid aerogels	Chemical reduction-supercritical drying	High conductivity of 7.5 S m^{-1}, large surface area of 435 m^2 g^{-1}, pore volume of 2.58 cm^3 g^{-1} and maximum desalination capacity of 633.3 mg g^{-1}.		Reprinted with permission from Sui Z, Meng Q, Zhang X, Ma R and Cao B 2012 Green synthesis of carbon nanotube-graphene hybrid aerogels and their use as versatile agents for water purification *J. Mater. Chem.* **22** 8767. Copyright (2012) by The Royal Society of Chemistry.	[119]
3D MoS$_2$/N-GAs	hydrothermal	High output current density of 0.36 mA cm^{-2} with a hydrogen production rate equal to 0.19 m^3 H$_2$/m^3 · d at 0.9 V bias		Reprinted with permission from Hou Y, Zhang B, Wen Z, Cui S, Guo X, He Z and Chen J 2014 A 3D hybrid of layered MoS$_2$/ nitrogen-doped graphene nanosheet aerogels: an effective catalyst for hydrogen evolution in microbial electrolysis cells *J. Mater. Chem.* A **2** 13795. Copyright (2014) by the Royal Society of Chemistry.	[120]
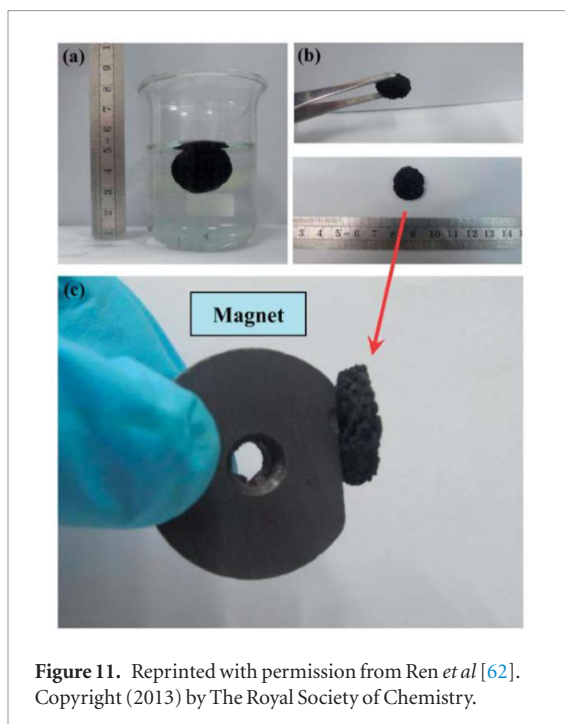
Figure 11. Reprinted with permission from Ren *et al* [62]. Copyright (2013) by The Royal Society of Chemistry.

Figure 12. Reprinted with permission from Song *et al* [64]. Copyright (2014) by Elsevier Ltd.

growth of mesoporous (2–50 nm) TiO_2 nanocrystals took place on GAs. The TiO_2/GA composites photocatalyzed methyl orange pollutant with high recyclability while they performed high specific capacity in LIBs. The high photocatalytic activity can be exploited in air purification and the enhanced specific capacity in fuel cells and supercapacitors. Si *et al* [126] synthesized a reduced GO aerogel (RGOA) through a simultaneous self-assembly and reduction method with hypophosphorous acid and iodine as reductant. The RGOA exhibited a high surface area of 830 $m^2\,g^{-1}$ and a high ability of supercapacitive performance in aqueous electrolytes, namely, 211.8 and 278.6 F g^{-1} in KOH and H_2SO_4. The latter characteristic is a result of the 3D structure and the presence of groups that contain oxygen. Wu *et al* [127] prepared a GA through a hydrogen reduction of GO aerogel (GOA) that was originated by GO solution and then was dried by supercritical drying. The final GA was found to have a high C/O molar ratio of 69.9 that makes this material an excellent candidate for supercapacitor applications. Wang *et al* [48] developed a solvothermal-induced self-assembly method to synthesize 3D Fe_2O_3 nanocubes/nitrogen-doped GA that can be used as anode materials for LIBs. The final aerogel, as an electrode material, exhibited high rate capability at high current densities (1140, 850, 640 and 420 mAh g^{-1} at 200, 1000, 3000, and 6000 mA g^{-1}, respectively) and remarkable cyclic stability (1121 mAh g^{-1} after 500 cycles at 500 mA g^{-1}).

Ren *et al* [62] reported a low-cost method for fabricating 3D free-standing nickel nanoparticle/GA with a graphene sheet network. The final product could be applied in ethanol fuel cells, since it shows a high peak current density at 6 mA cm^{-2} for ethanol oxidation under the test condition of adding 0.1 M ethanol in 0.1 M NaOH solution [62]. The final material comprises three important characteristics: firstly, Ni nanopar-

ticles which have good catalytic activity for ethanol electro-oxidation. Secondly, high electrical conductivity that ensures high current loads, and thirdly, the 3D porous graphene network enables maximum accessibility for active species and catalysts and enhances the mass transfer of reactants. In figure 11, a photo of the 3D aerogel is presented which shows that the material does not sink in water, is cylindrical, and has a diameter of about 20 mm.

Tan *et al* [47] synthesized tin dioxide nanoparticles on nitrogen doped GA (SnO_2-NGA) hybrid via a one-step hydrothermal process. Moreover, SnO_2-NGA hybrid exhibited a high lithium storage capacity of 1100 mAh g^{-1} after 100 cycles and this performance is believed to result from SnO_2 nanoparticles, a spongy structure and N doping defect for Li^+ diffusion. Chen *et al* [60] showed that three types of carbohydrates (glucose, β-cyclodextrin and chitosan) can enhance the structure, properties and the electrochemical performance of GBAs that were fabricated by a simple hydrothermal method. These materials could find appliation as supercapacitors, because after galvanostatic charge/discharge tests that were performed (with the GAs as electrodes), they showed with the addition of glucose, β-cyclodextrin and chitosan specific capacitances of 161.6, 130.1 and 89.3 F g^{-1}, respectively, at the current density of 0.5 A g^{-1}. 3D hierarchical porous graphene aerogel (HPGA) with uniform and tunable mesopores on graphene nanosheets (GNS) were prepared by Ren *et al* [128] also via a hydrothermal method, *in situ* carbothermal reaction and freeze drying. The material was examined as LIB anode and had a high reversible specific capacity of 1100 mAh g^{-1} at a current density of 0.1 A g^{-1}. Such behaviour is expected since the 3D macroporous structure with 2D mesoporous GNS favours adsorption, formation of thin graphitic layers for Li ion intercalation and a plethora of mesopores-cavities for maximizing the adsorption of Li ions.

Nitrogen doped graphene aerogel (NGA) has a 3D nanostructure, large surface area and remarkable mechanical properties [33]. A NGA has many sites for the nanoparticles to be dispersed, increases the binding force with the nanoparticles and so, it promotes lithium storage and transportation rate [63]. Song *et al* [64] developed an ultralight, 3D, nitrogen doped graphene aerogel (NGA) with the assistance of dopamine (DA), inspired by the marine mussel. The NGA (figure 12(a)) exhibited a density of 1.9 mg cm^{-3}, mechanical stabil-
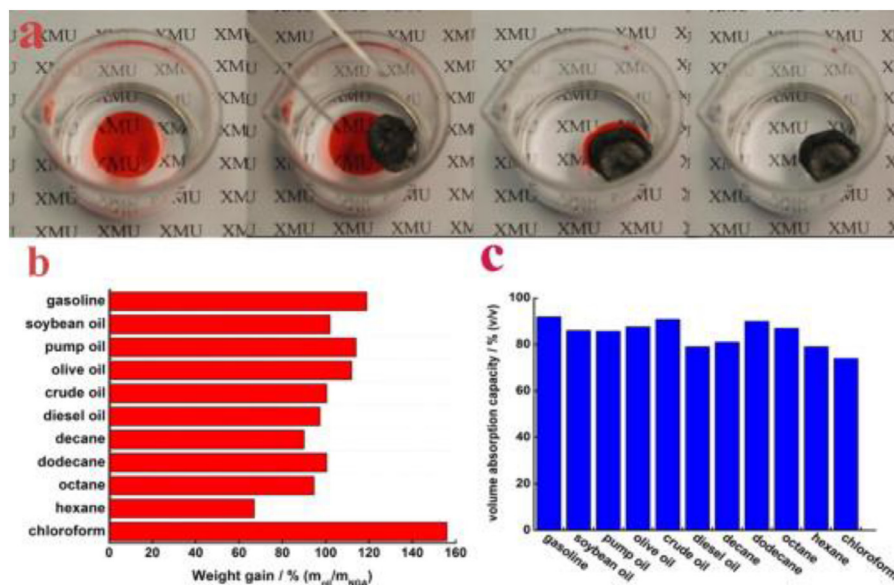
Figure 13. (a) NGA can absorb gasoline dyed with Sudan III. (b) Weight-based and (c) volume-based adsorption rates of the NGA (with density of 5.0 mg cm^{-3}) for oils and organic solvents. Reprinted with permission from Song *et al* [64]. Copyright (2014) by Elsevier Ltd.
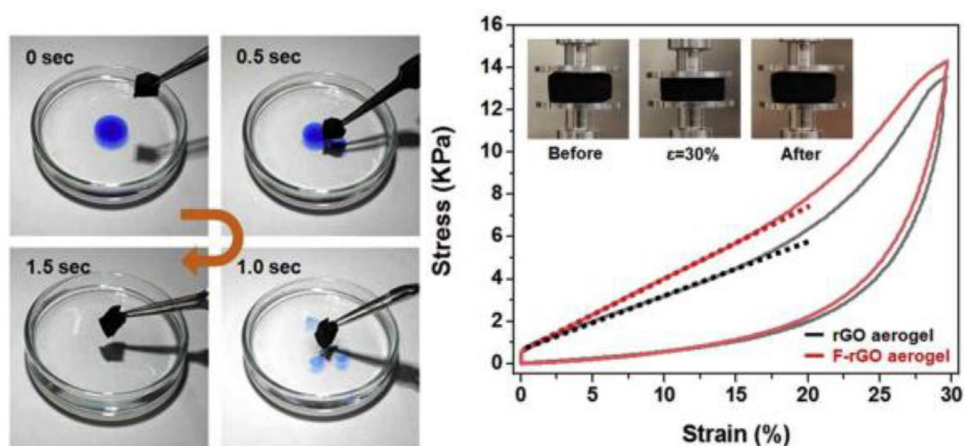

Figure 14. Left: Oil absorption test of the aerogel. Oil (stained with Oil blue N dye) floating on water was completely absorbed within 1.5 s. Right: Compressive stress–strain curves of the rGO aerogel (black) and Functionalized-rGO aerogel (red) performed by a dynamic mechanical analyzer with 30% strain in compression. Inset: images from before/after the 30% strain compression test. Reprinted with permission from Hong *et al* [129]. Copyright (2015) by Elsevier B.V.
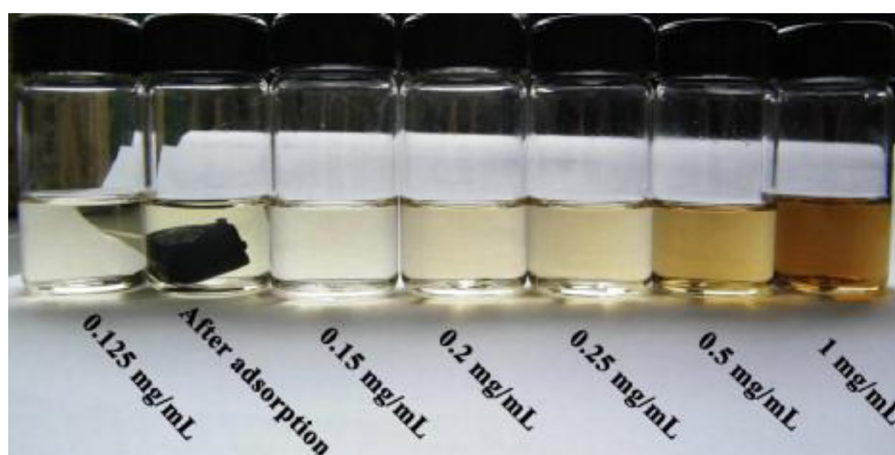
Figure 15. Photos of the crude oil solution for different concentrations and the crude oil solution (1 mg ml^{-1}) after the adsorption with RGA. Reprinted with permission from Li *et al* [130]. Copyright (2012) by Elsevier Inc.
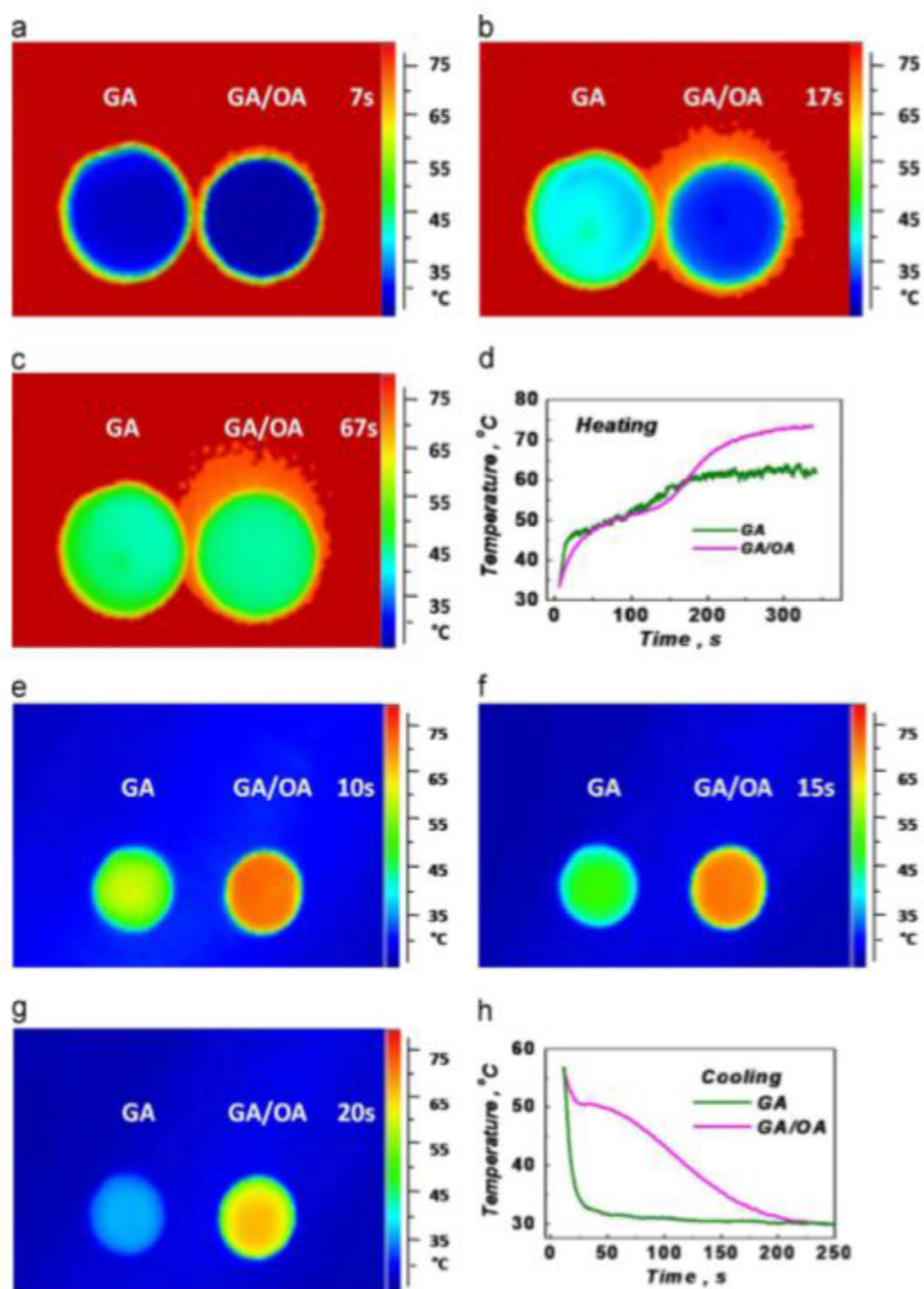
Figure 16. Thermal images and temperature responses of GAs and GA/OA composites during the heating time and during the cooling time. Reprinted with permission from Zhong *et al* [61]. Copyright (2013) by Elsevier B.V.
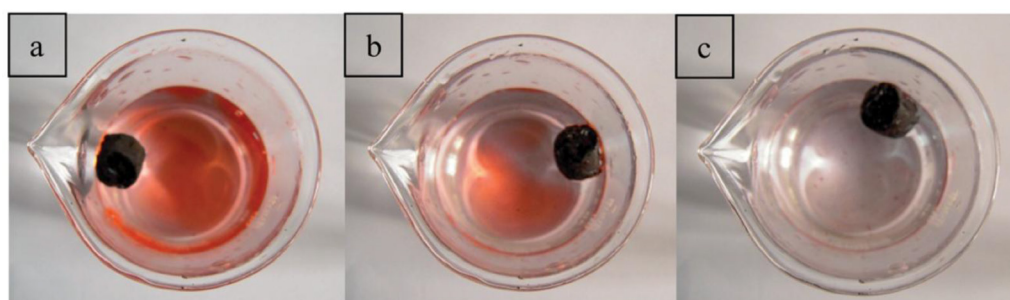
Figure 17. Photos of the absorption of diesel oil by GA over time (Sudan III was added to the oil for better observation) after 0, 1 and 4 min, respectively. Reprinted with permission from Wu *et al* [133]. Copyright (2013) by The Royal Society of Chemistry.

ity, fire resistance (figure 12(b)), high adsorption ability of oil (figure 13) and high conductivity that makes the aerogel a good candidate as electrode material for electrochemical sensors.

3.2. Environmental protection

Hong *et al* [129] prepared a functionalized GA with high porosity and hydrophobicity by surface treatment of self-assembled GOAs. The as-made GA exhibited a low density of 14.4 kg cm^{-3} and mechanical stability as it can stand 2600 times its own weight. Most importantly, this material has high absorption ability for several oils and organic solvents, and is regenerated with drying at above its melting point. Hence, it can be used for clearing spilled oils and other pollutants. This behaviour can be attributed to synergistic action of high porosity and high surface area which results from the 3D macroporous framework, and to close connection between hydrophobicity and oils-solvents. The regeneration capability is attributed to the strong network of the surface-modified GA that ensures chemical and mechanical durability. Figure 14 (left) shows the adsorption capacity of the GA for an oil blue N dye and figure 14 (right) shows the compressive stress–strain curve of the fluorinated GA. As shown, the compressive modulus from 24.9 kPa for rGO aerogel, increased to 34.6 kPa under 30% of compressive strain and this is attributed to the strong interactions between the rGO aerogel and the silane coupling agents.

Li *et al* [130] prepared a GA reinforced with tri-isocyanate. The reinforced GA (RGA) has a low bulk density equal to 0.08 g cm^{-3}, high compressive failure strength of 0.24 MPa and can absorb crude oil with a rate of $\approx$169 mg g^{-1}. In figure 15, the adsorption capacity of the material to crude oil is evident. In the adsorption test, 0.05 g of RGA was dispersed into 10 ml crude oil solution (1 mg ml^{-1} in n-octane). After 2 d at 35 °C, the concentration was $\approx$0.15 mg ml^{-1}. The high adsorption performance results from the high adsorption of graphene for organic molecules through π–π stacking interactions, and the highly porous structure of the RGA.

Han *et al* [131] prepared GAs of high mechanical strength (2.1 KPa), tunable density and volume through soaking graphene hydrogels in ammonia solution. The concentration of ammonia solution is crucial since it tailors the density and the volume of the GAs. The increase of the concentration induces a volume decrease but the macropore walls of the material become thicker. This increase gives a specific surface area of about 350 m^2 g^{-1} and larger porosity. Furthermore, it was found that the adsorption capacity of the GAs for Pb^{2+} from aqueous solution is approximately at 80 mg g^{-1} and reaches 5000 g m^{-3} per unit volume. It is obvious that these environmentally friendly materials can be used in waste water management, as well as, in energy conversion and storage. Zhong *et al* [61] reported the production of a composite phase change material (PCM) consisted of 3D GA and octadecanoic acid (OA). The aerogel was observed through a one step hydrothermal reaction. The
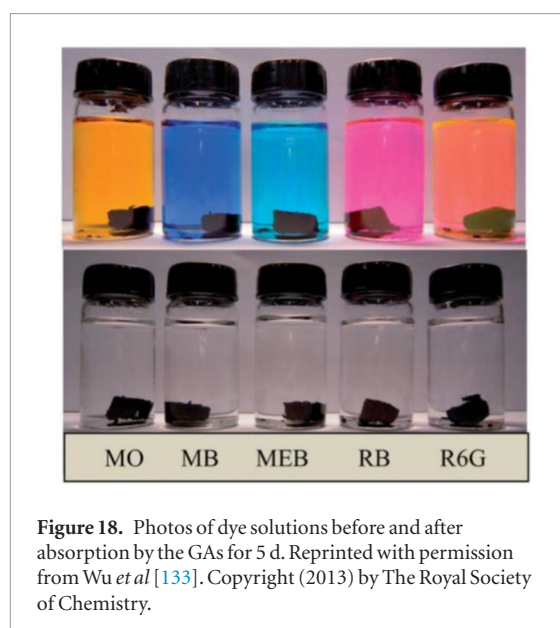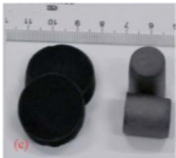

Figure 18. Photos of dye solutions before and after absorption by the GAs for 5 d. Reprinted with permission from Wu *et al* [133]. Copyright (2013) by The Royal Society of Chemistry.

composite material exhibited a thermal conductivity of 2.635 W m^{-1} · K^{-1} with a GA loading rate of $\approx$20 vol.%. High thermal conductivity of the GAs ligaments allows heat transfer throughout the OA, but also, GAs can stop the leakage of the molten PCM by capillary force. The heating and cooling responses of the GA/OA composite were examined for thermal energy storage and a high heat storage capacity of 181.8 J g^{-1} has been reported. Figure 16 shows thermal images and temperature responses of GAs and GA/OA composites during the heating cooling cycles, from which it is evident that the overall thermal behaviour of the composites was superior to a simple GA. Graphene fillers in PCMs matrix improve the thermal properties of the PCM composites, since they greatly reduce the internal contact thermal resistance in these materials. It has been found [1] that RT electrical conductivity of polymeric composites with GA fillers is increased by 1–6 orders of magnitude comparing to those with individual CNT or graphene fillers at a similar volume fraction.
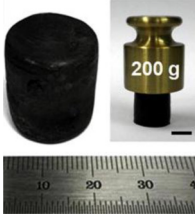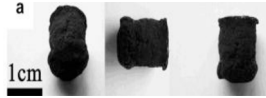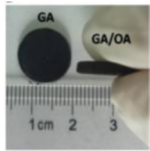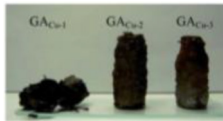
Zhao *et al* [132] synthesized a porous graphene oxide-chitosan aerogel (PGO-CS) with a hydrothermal method and lyophilization in order to use it as recyclable adsorbent for tetracycline removal. Tetracycline is an antibiotic which is an important pollutant of water. The adsorbing capacity of the PGO-CS is 1.47 × 103 mg g^{-1} and it was found that a higher pH and a higher ionic strength improve the adsorption. The adsorption behavior of the aerogel was simulated using several approaches. Wu *et al* [133] presented some synthesized GAs with good catalytic activity for the catalytic reduction of 4-nitrophenol, good photocatalytic degradation of methyl orange (MO) and capacity to remove oils and dyes from water. The GAs that were enriched with Cu nanoparticles, were developed through a reduction and self-assembly process, and then were dried via freezing. As it is shown in figure 17, these GAs have high absorption capacities for oils and dyes because of their porosity, hydrophobicity and their increased surface roughness. Also, as shown in figure 18, such a GA decolorized five kinds of dyes after 5 d such

Table 2. Concentrating table for GAs with their relative applications.

Aerogel name	Properties	Application	Photo		Reference
L-ascorbic acid aerogel	Specific capacitance of 128 F g^{-1}, can stand 14 000 times its weight	Electrodes for electrochemical power sources		Reprinted with permission from Zhang X, Sui Z, Xu B, Yue S, Luo Y, Zhan W and Liu B 2011 Mechanically strong and highly conductive graphene aerogel and its use as electrodes for electrochemical power sources *J. Mater. Chem.* **21** 6494. Copyright (2011) by The Royal Society of Chemistry.	[46]
TiO$_2$/GA	High porosity and high surface area, high recyclability and high specific capacity in LIBs	Electrode materials for LIBs and solar light photocatalysts, air purification, fuel cells and superca-pacitors		Reprinted with permission from Qiu B, Xing M and Zhang J 2014 Mesoporous TiO$_2$ nanocrystals grown *in situ* on graphene aerogels for high photocatalysis and lithium-ion batteries *J. Am. Chem. Soc.* **136** 5852. Copyright (2014) by the American Chemical Society.	[125]
3D Fe$_2$O$_3$ nanocubes/ nitrogen-doped GA	≈50 nm length, high high specific capacitance and high cyclic stability at high current densities	Anode materials for LIBs		Reprinted with permission from Wang R, Xu C, Sun J and Gao L 2014 Three-dimensional Fe$_2$O$_3$ nanocubes/ nitrogen-doped graphene aerogels: nucleation mechanism and lithium storage properties *Sci. Rep.* **4** 7171. Copyright (2014) by Nature Research.	[48]
3D free-standing nickel nanoparticle/ GA	High peak current density at 6 mA cm^{-2} for ethanol oxidation, diameter of about 20 mm	Ethanol fuel cells		Reprinted with permission from Ren L, Hui K S and Hui K N 2013 Self-assembled free-stand-ing 3D nickel nanoparticle/ graphene aerogel for direct ethanol fuel cells *J. Mater. Chem. A* **1** 5689. Copyright (2013) by The Royal Society of Chemistry.	[62]
SnO$_2$-NGA hybrid	High lithium storage capacity of 1100 mAh g^{-1} after 100 cycles	LIBs as free-stand-ing anode		Reprinted with permission from Tan C, Cao J, Khattak A M, Cai F, Jiang B, Yang G and Hu S 2014 *J. Power Sources* **270** 28. Copyright (2014) by Elsevier B.V.	[47]
3D hierarchical porous graphene aerogel (HPGA)	High reversible specific capacity of 1100 mAh g^{-1} at a current density of 0.1 A g^{-1}	LIB anode		Reprinted with permission from Ren L, Hui K N, Hui K S, Liu Y, Qi X, Zhong J, Du Y and Yang J 2015 Three-dimensional hierarchical porous graphene aerogel with tunable meso-pores on graphene nanosheets for high-performance energy storage *Sci. Rep.* **5** 14229. Copyright (2015) by Nature Research.	[128]
Nitrogen doped graphene aerogel (NGA)	Density of 1.9 mg cm^{-3}, mechani-cal stability, fire resistance, high adsorption ability of oil and high conductivity	Electrode material for electrochemical sensors		Reprinted with permission from Song X, Lin L, Rong M, Wang Y, Xie Z and Chen X 2014 Mussel-inspired, ultralight, multifunctional 3D nitrogen-doped graphene aerogel *Carbon* **80** 174. Copyright (2014) by Elsevier Ltd.	[64]

(*Continued*)

Table 2. (*Continued*)

Aerogel name	Properties	Application	Photo		Reference
Fluorinated GA	Density equal to 14.4 kg cm^{-3} and high mechanical stability: 2600 times its own weight, high absorption ability for several oils and organic solvents	Clearing spilled oils and other pollutants		Reprinted with permission from Hong J-Y, Sohn E-H, Park S and Park H S 2015 Highly-efficient and recyclable oil absorbing performance of functionalized graphene aerogel *Chem. Eng. J.* **269** 229. Copyright (2015) by Elsevier B.V.	[129]
Reinforced GA (RGA)	Low bulk density equal to 0.08 g cm^{-3}, high compressive failure strength of 0.24 MPa and high absorption of crude oil with a rate of $\approx$169 mg g^{-1}	Absorption of crude oil		Reprinted with permission from Li J, Wang F and Liu C-Y 2012 Tri-isocyanate reinforced graphene aerogel and its use for crude oil adsorption *J. Colloid Interface Sci.* **382** 13. Copyright (2012) by Elsevier Inc.	[130]
GAs-ammonia solution	Specific surface area of about 350 m^2 g^{-1}, adsorption capacity for Pb^{2+} equal to 5000 g m^{-3} per unit volume	Waste water management, energy conversion and storage.		Reprinted with permission from Han Z, Tang Z, Shen S, Zhao B, Zheng G and Yang J 2014 Strengthening of graphene aerogels with tunable density and high adsorption capacity towards Pb^{2+} *Sci. Rep.* **4** 5025. Copyright (2014) by Nature Research.	[131]
GA/ Octadecanoic acid	Thermal conductivity of 2.635 W m^{-1} · K^{-1} with a GA loading rate of $\approx$20 vol.%	Phase change material		Reprinted with permission from Zhong Y, Zhou M, Huang F, Lin T and Wan D 2013 Effect of graphene aerogel on thermal behavior of phase change materials for thermal management *Sol. Energy Mater. Sol. Cells* **113** 195. Copyright (2013) by Elsevier B.V.	[61]
Cu nanoparticles/ GAs	High absorption capacities for oils and dyes because of their porosity, hydrophobicity and surface roughness	Catalytic reduction of 4-nitrophenol, removal of several oils and dyes from water		Reprinted with permission from Wu T, Chen M, Zhang L, Xu X, Liu Y, Yan J, Wang W and Gao J 2013 Three-dimensional graphene-based aerogels prepared by a self-assembly process and its excellent catalytic and absorbing performance *J. Mater. Chem.* A **1** 7612. Copyright (2013) by The Royal Society of Chemistry.	[133]

as MO, methyl blue (MB), methylene blue (MEB), rhodamine B (RB) and rhodamine 6 G (R6G). The π–π interactions between the aerogel and the organic dyes are responsible for the observed behaviour. In table 2 current and future GA applications are listed.

4. Conclusions

In this review, a summary of recent progress on the synthesis methods and potential applications of GAs was presented. Regarding synthesis five most common methods were identified namely hydrothermal reduction, chemical reduction, cross-linking, sol–gel and template-directed reduction. The hydrothermal reduction method promotes the self-assembly of GNS, but conditions of high temperature/high pressure must be applied. The chemical reduction method uses mainly mild reduction agents to restore the sp^2 network but often leads to a small surface area since the graphene layers agglomerate through π–π interaction. In the sol–gel method, the bonding between GO sheets is stronger than the cross-linking method due to the formation of

covalent bonds between the sheets. Finally, the template-directed reduction can be a useful method to obtain porous GAs since it favours the creation of uniform macropores and tailorable microstructure. More recently 3D printing is also emerging as a promising processing route. It can be exploited to prepare GAs with several and complex shapes, and few layer graphene sheets can be traced in the aerogel, without flake aggregation.

GAs, due to their high surface area, high porosity, high electrical conductivity, high mechanical strength, thermal stability, high specific capacitance and high cyclic stability, are anticipated to be used as electrodes for electrochemical power sources and LIBs, and as supercapacitors. They can also be used in waste removal since they exhibit high adsorption capacity and photocatalytic ability for dyes, oils, organic solvents and inorganic ions. Other fields of potential use are as Phase Change Materials for better heating-cooling responses and as fire resistance agents.

GO, is the key constituent material but has some inherent drawbacks such as complex structure and random distribution of oxygen moieties on the surface, which could hamper the self-assembly of GNS. Other findings are related to concerns over the environmental footprint of GA drying processes and the related high cost, as compared to ambient-pressure drying for commercial silica aerogels. In future all these challenges must be dealt with in order to allow the laboratory synthesized GAs to enter commercial exploitation.

Acknowledgments

References

[1] Stankovich S *et al* 2006 Graphene-based composite materials *Nature* **442** 282–6

[2] Lee C *et al* 2008 Measurement of the elastic properties and intrinsic strength of monolayer graphene *Science* **321** 385–8

[3] Peigney A *et al* 2001 Specific surface area of carbon nanotubes and bundles of carbon nanotubes *Carbon* **39** 507–14

[4] Balandin A A *et al* 2008 Superior thermal conductivity of single-layer graphene *Nano Lett.* **8** 902–7

[5] Ramanathan T *et al* 2008 Functionalized graphene sheets for polymer nanocomposites *Nat. Nano* **3** 327–31

[6] Vickery J L, Patil A J and Mann S 2009 Fabrication of graphene–polymer nanocomposites with higher-order three-dimensional architectures *Adv. Mater.* **21** 2180–4

[7] Eda G and Chhowalla M 2009 Graphene-based composite thin films for electronics *Nano Lett.* **9** 814–8

[8] Eda G, Fanchini G and Chhowalla M 2008 Large-area ultrathin films of reduced graphene oxide as a transparent and flexible electronic material *Nat. Nano* **3** 270–4

[9] Wang X, Zhi L and Müllen K 2008 Transparent, conductive graphene electrodes for dye-sensitized solar cells *Nano Lett.* **8** 323–7

[10] Yoo E *et al* 2008 Large reversible Li storage of graphene nanosheet families for use in rechargeable lithium ion batteries *Nano Lett.* **8** 2277–82

[11] Schedin F *et al* 2007 Detection of individual gas molecules adsorbed on graphene *Nat. Mater.* **6** 652–5

[12] Shao Y *et al* 2010 Graphene based electrochemical sensors and biosensors: a review *Electroanalysis* **22** 1027–36

[13] Sutter P W, Flege J-I and Sutter E A 2008 Epitaxial graphene on ruthenium *Nat. Mater.* **7** 406–11

[14] Menaa F, Abdelghani A and Menaa B 2015 Graphene nanomaterials as biocompatible and conductive scaffolds for stem cells: impact for tissue engineering and regenerative medicine *J. Tissue Eng. Regen. Med.* **9** 1321–38

[15] Gu Y, Xu Y and Wang Y 2013 Graphene-wrapped CoS nanoparticles for high-capacity lithium-ion storage *ACS Appl. Mater. Interfaces* **5** 801–6

[16] Ju S A *et al* 2011 Graphene-wrapped hybrid spheres of electrical conductivity *ACS Appl. Mater. Interfaces* **3** 2904–11

[17] Zhang H-B *et al* 2011 Tough graphene-polymer microcellular foams for electromagnetic interference shielding *ACS Appl. Mater. Interfaces* **3** 918–24

[18] Zhang H-B *et al* 2010 Electrically conductive polyethylene terephthalate/graphene nanocomposites prepared by melt compounding *Polymer* **51** 1191–6

[19] Zhang S *et al* 2011 Graphene-polypyrrole nanocomposite as a highly efficient and low cost electrically switched ion exchanger for removing from wastewater *ACS Appl. Mater. Interfaces* **3** 3633–7

[20] Wang Y *et al* 2011 Super-elastic graphene ripples for flexible strain sensors *ACS Nano* **5** 3645–50

[21] Zhu Y *et al* 2010 Graphene and graphene oxide: synthesis, properties, and applications *Adv. Mater.* **22** 3906–24

[22] Rao C N R *et al* 2009 Graphene: the new two-dimensional nanomaterial *Angew. Chem., Int. Ed.* **48** 7752–77

[23] Liang J *et al* 2009 Electromagnetic interference shielding of graphene/epoxy composites *Carbon* **47** 922–5

[24] Kim H, Miura Y and Macosko C W 2010 Graphene/polyurethane nanocomposites for improved gas barrier and electrical conductivity *Chem. Mater.* **22** 3441–50

[25] Cong H-P *et al* 2012 Macroscopic multifunctional graphene-based hydrogels and aerogels by a metal ion induced self-assembly process *ACS Nano* **6** 2693–703

[26] Wu C *et al* 2013 Mechanically flexible and multifunctional polymer-based graphene foams for elastic conductors and oil-water separators *Adv. Mater.* **25** 5658–62

[27] Chen C *et al* 2009 Self-assembled free-standing graphite oxide membrane *Adv. Mater.* **21** 3007–11

[28] Chen H *et al* 2008 Mechanically strong, electrically conductive, and biocompatible graphene paper *Adv. Mater.* **20** 3557–61

[29] Chen J *et al* 2012 Graphene hydrogels deposited in nickel foams for high-rate electrochemical capacitors *Adv. Mater.* **24** 4569–73

[30] Chen W *et al* 2011 Self-assembly and embedding of nanoparticles by *in situ* reduced graphene for preparation of a 3D graphene/nanoparticle aerogel *Adv. Mater.* **23** 5679–83

[31] Sun H, Xu Z and Gao C 2013 Multifunctional, ultra-flyweight, synergistically assembled carbon aerogels *Adv. Mater.* **25** 2554–60

[32] Xu Y *et al* 2009 Strong and ductile poly(vinyl alcohol)/graphene oxide composite films with a layered structure *Carbon* **47** 3538–43

[33] Xu Y *et al* 2010 Self-assembled graphene hydrogel via a one-step hydrothermal process *ACS Nano* **4** 4324–30

[34] Nardecchia S *et al* 2013 Three dimensional macroporous architectures and aerogels built of carbon nanotubes and/or graphene: synthesis and applications *Chem. Soc. Rev.* **42** 794–830

[35] Qian Y I, Ismail M and Stein A 2014 Ultralight, high-surface-area, multifunctional graphene-based aerogels from self-assembly of graphene oxide and resol *Carbon* **68** 221–31

[36] Zaman I *et al* 2012 From carbon nanotubes and silicate layers to graphene platelets for polymer nanocomposites *Nanoscale* **4** 4578–86

[37] Miller S G *et al* 2010 Characterization of epoxy functionalized graphite nanoparticles and the physical properties of epoxy matrix nanocomposites *Compos. Sci. Technol.* **70** 1120–5

[38] Qin Z *et al* 2017 The mechanics and design of a lightweight three-dimensional graphene assembly *Sci. Adv.* **3** e1601536

[39] Gorgolis G and Karamanis D 2016 Solar energy materials for glazing technologies *Sol. Energy Mater. Sol. Cells* **144** 559–78

[40] Pierre A C and Pajonk G M 2002 Chemistry of aerogels and their applications *Chem. Rev.* **102** 4243–66

[41] Hao G-P *et al* 2010 Rapid synthesis of nitrogen-doped porous carbon monolith for CO_2 capture *Adv. Mater.* **22** 853–7

[42] Tao Y, Endo M and Kaneko K 2009 Hydrophilicity-controlled carbon aerogels with high mesoporosity *J. Am. Chem. Soc.* **131** 904–5

[43] Yoshizawa N *et al* 2003 Structure and electrochemical properties of carbon aerogels polymerized in the presence of Cu^{2+} *J. Non-Cryst. Solids* **330** 99–105

[44] Meng F *et al* 2011 Alkali-treated graphene oxide as a solid base catalyst: synthesis and electrochemical capacitance of graphene/carbon composite aerogels *J. Mater. Chem.* **21** 18537–9

[45] Wu Z-S *et al* 2012 Three-dimensional nitrogen and boron Co-doped graphene for high-performance all-solid-state supercapacitors *Adv. Mater.* **24** 5130–5

[46] Zhang X *et al* 2011 Mechanically strong and highly conductive graphene aerogel and its use as electrodes for electrochemical power sources *J. Mater. Chem.* **21** 6494–7

[47] Tan C *et al* 2014 High-performance tin oxide-nitrogen doped graphene aerogel hybrids as anode materials for lithium-ion batteries *J. Power Sources* **270** 28–33

[48] Wang R *et al* 2014 Three-dimensional Fe_2O_3 nanocubes/nitrogen-doped graphene aerogels: nucleation mechanism and lithium storage properties *Sci. Rep.* **4** 7171

[49] Narasimman R and Prabhakaran K 2013 Preparation of carbon foams with enhanced oxidation resistance by foaming molten sucrose using a boric acid blowing agent *Carbon* **55** 305–12

[50] Py X, Olives R and Mauran S 2001 Paraffin/porous-graphite-matrix composite as a high and constant power thermal storage material *Int. J. Heat Mass Transfer* **44** 2727–37

[51] Zhong Y *et al* 2010 Heat transfer enhancement of paraffin wax using compressed expanded natural graphite for thermal energy storage *Carbon* **48** 300–4

[52] De Leon C P and Pletcher D 1995 Removal of formaldehyde from aqueous solutions via oxygen reduction using a reticulated vitreous carbon cathode cell *J. Appl. Electrochem.* **25** 307–14

[53] Harikrishnan G, Patro T U and Khakhar D V 2007 Reticulated vitreous carbon from polyurethane foam–clay composites *Carbon* **45** 531–5

[54] Pham H D *et al* 2011 Synthesis of the chemically converted graphene xerogel with superior electrical conductivity *Chem. Commun.* **47** 9672–4

[55] Bi H *et al* 2012 Low temperature casting of graphene with high compressive strength *Adv. Mater.* **24** 5124–9

[56] Chen Z *et al* 2011 Three-dimensional flexible and conductive interconnected graphene networks grown by chemical vapour deposition *Nat. Mater.* **10** 424–8

[57] Mesalhy O, Lafdi K and Elgafy A 2006 Carbon foam matrices saturated with PCM for thermal protection purposes *Carbon* **44** 2080–8

[58] Alrashdan A, Mayyas A T and Al-Hallaj S 2010 Thermo-mechanical behaviors of the expanded graphite-phase change material matrix used for thermal management of Li-ion battery packs *J. Mater. Process. Technol.* **210** 174–9

[59] Xiang J and Drzal L T 2011 Investigation of exfoliated graphite nanoplatelets (*x*GnP) in improving thermal conductivity of paraffin wax-based phase change material *Sol. Energy Mater. Sol. Cells* **95** 1811–8

[60] Ji C-C *et al* 2013 Self-assembly of three-dimensional interconnected graphene-based aerogels and its application in supercapacitors *J. Colloid Interface Sci.* **407** 416–24

[61] Zhong Y *et al* 2013 Effect of graphene aerogel on thermal behavior of phase change materials for thermal management *Sol. Energy Mater. Sol. Cells* **113** 195–200

[62] Ren L, Hui K S and Hui K N 2013 Self-assembled free-standing three-dimensional nickel nanoparticle/graphene aerogel for direct ethanol fuel cells *J. Mater. Chem.* A **1** 5689–94

[63] Reddy A L M *et al* 2010 Synthesis of nitrogen-doped graphene films for lithium battery application *ACS Nano* **4** 6337–42

[64] Song X *et al* 2014 Mussel-inspired, ultralight, multifunctional 3D nitrogen-doped graphene aerogel *Carbon* **80** 174–82

[65] Dreyer D R *et al* 2010 The chemistry of graphene oxide *Chem. Soc. Rev.* **39** 228–40

[66] Kim F, Cote L J and Huang J 2010 Graphene oxide: surface activity and two-dimensional assembly *Adv. Mater.* **22** 1954–8

[67] Kim J *et al* 2010 Graphene oxide sheets at interfaces *J. Am. Chem. Soc.* **132** 8180–6

[68] Bai H *et al* 2011 Graphene oxide/conducting polymer composite hydrogels *J. Mater. Chem.* **21** 18653–8

[69] Zu S-Z and Han B-H 2009 Aqueous dispersion of graphene sheets stabilized by pluronic copolymers: formation of supramolecular hydrogel *J. Phys. Chem.* C **113** 13651–7

[70] Ma X *et al* 2013 Temperature-sensitive poly(N-isopropylacrylamide)/graphene oxide nanocomposite hydrogels by *in situ* polymerization with improved swelling capability and mechanical behavior *Eur. Polym. J.* **49** 389–96

[71] Liu J, Chen G and Jiang M 2011 Supramolecular hybrid hydrogels from noncovalently functionalized graphene with block copolymers *Macromolecules* **44** 7682–91

[72] Worsley M A *et al* 2010 Synthesis of graphene aerogel with high electrical conductivity *J. Am. Chem. Soc.* **132** 14067–9

[73] Chen C-M *et al* 2012 Macroporous 'bubble' graphene film via template-directed ordered-assembly for high rate supercapacitors *Chem. Commun.* **48** 7149–51

[74] Wang Z *et al* 2016 Ultralow electrical percolation in graphene aerogel/epoxy composites *Chem. Mater.* **28** 6731–41

[75] Cao J *et al* 2013 Enhanced activity of Pd nanoparticles supported on Vulcan XC72R carbon pretreated via a modified Hummers method for formic acid electrooxidation *Appl. Surf. Sci.* **274** 138–43

[76] Wu Z-S *et al* 2012 3D nitrogen-doped graphene aerogel-supported Fe_3O_4 nanoparticles as efficient electrocatalysts for the oxygen reduction reaction *J. Am. Chem. Soc.* **134** 9082–5

[77] Zhang L *et al* 2015 3D porous hybrids of defect-rich MoS_2/graphene nanosheets with excellent electrochemical performance as anode materials for lithium ion batteries *RSC Adv.* **5** 34777–87

[78] Worsley M A *et al* 2014 Synthesis and characterization of highly crystalline graphene aerogels *ACS Nano* **8** 11013–22

[79] Goldstein A P *et al* 2014 Simultaneous sheet cross-linking and deoxygenation in the graphene oxide sol–gel transition *J. Phys. Chem.* C **118** 28855–60

[80] Worsley M A *et al* 2011 High surface area, sp2-cross-linked three-dimensional graphene monoliths *J. Phys. Chem. Lett.* **2** 921–5

[81] Sheng K-X *et al* 2011 High-performance self-assembled graphene hydrogels prepared by chemical reduction of graphene oxide *New Carbon Mater.* **26** 9–15

[82] Pei S *et al* 2010 Direct reduction of graphene oxide films into highly conductive and flexible graphene films by hydrohalic acids *Carbon* **48** 4466–74

[83] Moon I K *et al* 2010 Reduced graphene oxide by chemical graphitization *Nat. Commun.* **1** 73

[84] Park S *et al* 2011 Hydrazine-reduction of graphite- and graphene oxide *Carbon* **49** 3019–23

[85] Chen W and Yan L 2011 *In situ* self-assembly of mild chemical reduction graphene for three-dimensional architectures *Nanoscale* **3** 3132–7

[86] Worsley M A *et al* 2012 Mechanically robust 3D graphene macroassembly with high surface area *Chem. Commun.* **48** 8428–30

[87] Zhang L *et al* 2012 Three-dimensional assemblies of graphene prepared by a novel chemical reduction-induced self-assembly method *Nanoscale* **4** 7038–45

[88] Chen M *et al* 2013 A one-step method for reduction and self-assembling of graphene oxide into reduced graphene oxide aerogels *J. Mater. Chem.* A **1** 2869–77

[89] Parvez K *et al* 2014 Exfoliation of graphite into graphene in aqueous solutions of inorganic salts *J. Am. Chem. Soc.* **136** 6083–91

[90] Singh V V *et al* 2012 Greener electrochemical synthesis of high quality graphene nanosheets directly from pencil and its SPR sensing application *Adv. Funct. Mater.* **22** 2352–62

[91] Liu F and Xue D 2015 Advanced graphene nanomaterials for electrochemical energy storage *Mater. Res. Innov.* **19** 7–19

[92] Liu F and Xue D 2015 Electrochemical energy storage applications of 'pristine' graphene produced by non-oxidative routes *Sci. China Technol. Sci.* **58** 1841–50

[93] Chen K and Xue D 2015 *In situ* electrochemical route to aerogel electrode materials of graphene and hexagonal CeO_2 *J. Colloid Interface Sci.* **446** 77–83

[94] Bai H *et al* 2011 On the gelation of graphene oxide *J. Phys. Chem.* C **115** 5545–51

[95] Everett D H 1988 *Basic Principles of Colloid Science* (London: The Royal Society of Chemistry)

[96] Hu H *et al* 2013 Ultralight and highly compressible graphene aerogels *Adv. Mater.* **25** 2219–23

[97] Jiang X *et al* 2010 Self-assembly of reduced graphene oxide into three-dimensional architecture by divalent ion linkage *J. Phys. Chem.* C **114** 22462–5

[98] Choi B G *et al* 2012 3D macroporous graphene frameworks for supercapacitors with high energy and power densities *ACS Nano* **6** 4020–8

[99] Estevez L *et al* 2011 Multifunctional graphene/platinum/nafion hybrids via ice templating *J. Am. Chem. Soc.* **133** 6122–5

[100] Lin Y *et al* 2016 Pristine graphene aerogels by room-temperature freeze gelation *Adv. Mater.* **28** 7993–8000

[101] Araki K and Halloran J W 2004 New freeze-casting technique for ceramics with sublimable vehicles *J. Am. Ceram. Soc.* **87** 1859–63

[102] Araki K and Halloran J W 2004 Room-temperature freeze casting for ceramics with nonaqueous sublimable vehicles in the naphthalene–camphor eutectic system *J. Am. Ceram. Soc.* **87** 2014–9

[103] Araki K and Halloran J W 2005 Porous ceramic bodies with interconnected pore channels by a novel freeze casting technique *J. Am. Ceram. Soc.* **88** 1108–14

[104] Barg S *et al* 2014 Mesoscale assembly of chemically modified graphene into complex cellular networks *Nat. Commun.* **5** 4328

[105] García-Tuñon E *et al* 2015 Printing in three dimensions with graphene *Adv. Mater.* **27** 1688–93

[106] Zhu C *et al* 2015 Highly compressible 3D periodic graphene aerogel microlattices *Nat. Commun.* **6** 6962

[107] Qiu L *et al* 2012 Biomimetic superelastic graphene-based cellular monoliths *Nat. Commun.* **3** 1241

[108] Sui Z-Y *et al* 2015 Nitrogen-doped graphene aerogels as efficient supercapacitor electrodes and gas adsorbents *ACS Appl. Mater. Interfaces* **7** 1431–8

[109] Worsley M A *et al* 2009 Mechanically robust and electrically conductive carbon nanotube foams *Appl. Phys. Lett.* **94** 073115

[110] Lewis J A 2006 Direct ink writing of 3D functional materials *Adv. Funct. Mater.* **16** 2193–204

[111] Worsley M A *et al* 2014 Toward macroscale, isotropic carbons with graphene-sheet-like electrical and mechanical properties *Adv. Funct. Mater.* **24** 4259–64

[112] Pekala R W, Alviso C T and LeMay J D 1990 Organic aerogels: microstructural dependence of mechanical properties in compression *J. Non-Cryst. Solids* **125** 67–75

[113] Tang Z *et al* 2010 Noble-metal-promoted three-dimensional macroassembly of single-layered graphene oxide *Angew. Chem., Int. Ed.* **49** 4603–7

[114] Kim K H, Oh Y and Islam M F 2012 Graphene coating makes carbon nanotube aerogels superelastic and resistant to fatigue *Nat. Nano* **7** 562–6

[115] Si Y *et al* 2014 Ultralight nanofibre-assembled cellular aerogels with superelasticity and multifunctionality *Nat. Commun.* **5** 5802

[116] Scaffaro R *et al* 2016 Synthesis and self-assembly of a PEGylated-graphene aerogel *Compos. Sci. Technol.* **128** 193–200

[117] Li J *et al* 2007 Correlations between percolation threshold, dispersion state, and aspect ratio of carbon nanotubes *Adv. Funct. Mater.* **17** 3207–15

[118] Wei G *et al* 2013 Ni-doped graphene/carbon cryogels and their applications as versatile sorbents for water purification *ACS Appl. Mater. Interfaces* **5** 7584–91

[119] Sui Z *et al* 2012 Green synthesis of carbon nanotube-graphene hybrid aerogels and their use as versatile agents for water purification *J. Mater. Chem.* **22** 8767–71

[120] Hou Y *et al* 2014 A 3D hybrid of layered MoS_2/nitrogen-doped graphene nanosheet aerogels: an effective catalyst for hydrogen evolution in microbial electrolysis cells *J. Mater. Chem.* A **2** 13795–800

[121] Zhang Y *et al* 2015 Graphene/carbon aerogels derived from graphene crosslinked polyimide as electrode materials for supercapacitors *RSC Adv.* **5** 1301–8

[122] Zuo L *et al* 2017 Graphene/montmorillonite hybrid synergistically reinforced polyimide composite aerogels with enhanced flame-retardant performance *Compos. Sci. Technol.* **139** 57–63

[123] Wang Z *et al* 2016 *17th European Conf. on Composite Materials Munich (Germany, 26–30 June 2016)*

[124] Bryning M B *et al* 2007 Carbon nanotube aerogels *Adv. Mater.* **19** 661–4

[125] Qiu B, Xing M and Zhang J 2014 Mesoporous TiO_2 nanocrystals grown *in situ* on graphene aerogels for high photocatalysis and lithium-ion batteries *J. Am. Chem. Soc.* **136** 5852–5

[126] Si W *et al* 2013 Reduced graphene oxide aerogel with high-rate supercapacitive performance in aqueous electrolytes *Nanoscale Res. Lett.* **8** 247

[127] Wu X *et al* 2012 High-rate capacitive performance of graphene aerogel with a superhigh C/O molar ratio *J. Mater. Chem.* **22** 23186–93

[128] Ren L *et al* 2015 3D hierarchical porous graphene aerogel with tunable meso-pores on graphene nanosheets for high-performance energy storage *Sci. Rep.* **5** 14229

[129] Hong J-Y *et al* 2015 Highly-efficient and recyclable oil absorbing performance of functionalized graphene aerogel *Chem. Eng. J.* **269** 229–35

[130] Li J, Wang F and Liu C-Y 2012 Tri-isocyanate reinforced graphene aerogel and its use for crude oil adsorption *J. Colloid Interface Sci.* **382** 13–6

[131] Han Z *et al* 2014 Strengthening of graphene aerogels with tunable density and high adsorption capacity towards Pb^{2+} *Sci. Rep.* **4** 5025

[132] Zhao L, Dong P, Xie J, Li J, Wu X, Yang S-T and Luo J 2013 Porous graphene oxide–chitosan aerogel for tetracycline removal *Mater. Res. Express* **1** 015601

[133] Wu T *et al* 2013 Three-dimensional graphene-based aerogels prepared by a self-assembly process and its excellent catalytic and absorbing performance *J. Mater. Chem.* A **1** 7612–21